Annu. Rev. Phys. Chem. 2003. 54:331–66
doi: 10.1146/annurev.physchem.54.011002.103759

First published online as a Review in Advance on March 4, 2003

OPTICAL PROPERTIES AND ULTRAFAST DYNAMICS OF METALLIC NANOCRYSTALS

Stephan Link and Mostafa A. El-Sayed
Laser Dynamics Laboratory, School of Chemistry and Biochemistry, Atlanta, Georgia 30332-0400; email: Mostafa.el-sayed@chemistry.gatech.edu

Key Words nanoparticles, femtosecond, plasmon

■ **Abstract** Noble metal particles have long fascinated scientists because of their intense color, which led to their application in stained glass windows as early as the Middle Ages. The recent resurrection of colloidal and cluster chemistry has brought about the strive for new materials that allow a bottoms-up approach of building improved and new devices with nanoparticles or artificial atoms. In this review, we discuss some of the properties of individual and some assembled metallic nanoparticles with a focus on their interaction with cw and pulsed laser light of different energies. The potential application of the plasmon resonance as sensors is discussed.

INTRODUCTION

As a consequence of reducing the size and the dimensionality of a material, its electronic properties change drastically as the density of states and the spatial length scale of the electronic motion are reduced with decreasing size. The energy eigenstates are now determined by the system's boundaries, and therefore surface effects become very important. A transition from the bulk band structure to individual localized energy levels occurs in clusters of subnanometer to nanometer size, and the detection of quantum size effects has been of great interest to scientists and technologists in the search for novel materials with exciting new properties (1–9a,b,c). Possible future applications of nanoparticles include the areas of ultrafast data communication and optical data storage (10–12), solar energy conversion (13), and the use of metallic nanoparticles as catalysts (14–16) because of their high surface-to-volume ratios and different shapes (9c).

Closely related to size-induced changes in the electronic structure are the optical properties of nanoparticles. Spectroscopic methods probe the energy differences between two states for allowed transitions as well as the lifetimes of excited states and their respective energy relaxation channels using time-resolved techniques. The size effect on the optical absorption spectra of metallic nanocrystals is probably best known for the noble metal nanoparticles (17–20). Indeed, metallic nanoparticles have fascinated scientists since the Middle Ages because of their colorful

colloidal solutions (21). Gold nanoparticles were used as a pigment of ruby-colored stained glass dating back to the seventeenth century. Figure 1 shows a picture of the Rose Window of the Cathedral of Notre Dame. The bright red and purple colors are due to gold nanoparticles. Faraday (22) first recognized this phenomenon, and Mie (23) was able to explain it theoretically in 1908 by solving Maxwell's equation. The physical origin of the strong light absorption by noble metal nanoparticles is the coherent oscillation of the conduction band electrons induced by interaction with an electromagnetic field. These resonances are known as surface plasmons (17–20) and are a small particle as well as a surface effect because they are absent in the individual atoms as well as in the bulk. Their extinction coefficient scales with the volume of the particles and can reach values several orders of magnitude larger compared to common organic dye molecules (9a,b,c).

Whereas the knowledge of the electronic and optical properties of a collection of individual well-separated particles is of fundamental scientific interest, the even greater flexibility in designing tailored properties of organized nanostructures has stimulated research for building new materials and devices with nanoparticles or artificial atoms as their building blocks (5, 24–27). The overall properties of the new material are determined by the properties of the individual particles as a function of their size and shape as well as their collective behavior. The latter is controlled by the interparticle separations, which can be changed by the size of the stabilizing ligands (capping material) protecting the particles against aggregation (28). Both parameters can now be manipulated by chemists in an ever-increasing degree, opening the possibilities for a bottoms-up approach toward the fabrication of new materials (24–28).

This review focuses on the properties of metallic nanoparticles. Optical properties of the noble metals, which directly reflect the size-dependent energy structure of the particles, are chosen as an example. The origin of the plasmon absorption and its theoretical treatment for different sizes and shapes are discussed. Time-resolved spectroscopies reveal the dynamics of the electrons in confined metallic systems, and the interaction with intense laser beams allows the synthesis as well as the size-selective reshaping of metallic nanoparticles. The optical properties of assembled particles and some of their assembly methods are discussed. As examples for the application of metallic nanoparticles, the area of sensors was chosen. Special emphasis has been placed on including the most recent results in this fast growing field, hence sacrificing completeness in other related areas. Especially interesting advances in the single-particle spectroscopy of metallic nanoparticles have been included by which problems associated with the inherent size and shape distribution of metallic nanoparticles can be circumvented. The plasmon absorption spectrum of single nanoparticles are now studied, which allows us to draw conclusions about the effect of its environment as well as the decay mechanism of the plasmon resonance. Surface enhanced Raman spectroscopy (SERS) on single particles furthermore sheds new light onto this powerful technique while also giving rise to new questions concerning the enhancement mechanism in SERS.

Because of the space limitation, preparative methods and magnetic and catalytic properties are not included.

THE SURFACE PLASMON RESONANCE

The intense color of colloidal noble metal particles in stained glass windows as illustrated in Figure 1 is caused by the surface plasmon resonance. The surface plasmon resonance can be thought of as the coherent motion of the conduction-band electrons caused by interaction with an electromagnetic field (17–20). In a classical description, the electric field of an incoming light wave induces a polarization of the electrons with respect to the much heavier ionic core of a spherical nanoparticle. A net charge difference is only felt at the nanoparticle surface, which in turn acts as a restoring force. This creates, in the simplest case, a dipolar oscillation of all the electrons with the same phase. When the frequency of the electromagnetic field becomes resonant with the coherent electron motion, a strong absorption in the spectrum is seen, which is the origin of the observed color. The frequency and width of the surface plasmon absorption depend on the size and shape of the metal nanoparticle as well as on the dielectric constant of the metal itself and of the medium surrounding it (17–20). The plasmon resonance is strongest and shifted into the visible part of the electromagnetic spectrum for the noble metals [copper, silver, and gold (29)], which is the reason why the noble metals have historically fascinated scientists dating back as early as Faraday (22). Most other transition metals only show a broad and poorly resolved absorption band in the ultraviolet (29). This difference can be attributed to the strong coupling between the plasmon transition and the interband excitation and to the fact that the conduction-band electrons of the noble metals can be well approximated by the Drude free-electron model (30). This model assumes that the conduction-band electrons can be treated independently from the ionic background and can move "freely," whereas the ions only act as scattering centers. This in turn gives the electrons in the noble metals a higher polarizability, thereby shifting the plasmon resonance to lower frequencies and also giving rise to a sharp bandwidth.

The linear optical properties like extinction and scattering of small spherical metal particles accounting for the surface plasmon resonance were explained theoretically by the groundbreaking work of Mie in 1908 (23). Mie solved Maxwell's equation for an electromagnetic light wave interacting with a small sphere having the same macroscopic, frequency-dependent material dielectric constant as the bulk metal. With the appropriate boundary conditions for a spherical object, his electrodynamic calculations gave a series of multipole oscillations (dipole, quadrupole, etc.) for the extinction and scattering cross section of the particles as a function of the particle radius. For large nanoparticles (>20 nm), the absorption spectrum is then composed of the sum of absorption and scattering modes, each of which has a contribution that depends on the particle size. Higher-order modes become more dominant with increasing particle size causing the plasmon absorption band to redshift while the bandwidth increases. Physically, this can be

explained by the fact that for larger particles the light cannot polarize the nanoparticles homogeneously and retardation effects lead to the excitation of higher-order modes (17). As the optical absorption spectra depend directly on the size of the nanoparticles, this is regarded as an extrinsic size effect (17). In this size regime, Mie's theory and experimental spectra agree well until for bulk metals the normal incidence absorption no longer shows a plasmon resonance.

For nanoparticles much smaller than the wavelength (<20 nm) of the interacting light only the dipole oscillation contributes significantly to the extinction cross section. Mie's theory then reduces to the following expression (dipole approximation) (17–20):

$$\sigma_{ext} = \frac{9 \cdot V \cdot \varepsilon_m^{3/2}}{c} \cdot \frac{\omega \cdot \varepsilon_2(\omega)}{[\varepsilon_1(\omega) + 2 \cdot \varepsilon_m]^2 + \varepsilon_2(\omega)^2}. \quad 1.$$

V is the particle volume, ω is the angular frequency of the exciting light, and c is the speed of light. ε_m and $\varepsilon(\omega) = \varepsilon_1(\omega) + i\varepsilon_2(\omega)$ are the dielectric functions of the surrounding medium and the metal, respectively. For the metal, the dielectric function is complex and depends on the frequency. The resonance condition is fulfilled roughly when $\varepsilon_1(\omega) = -2 * \varepsilon_m$ if ε_2 is small or weakly dependent on ω.

Within the dipole approximation (Equation 1) the surface plasmon resonance is independent of the particle size. This is in strong contradiction with experimental results on metallic nanoparticles much smaller than 10 nm (17). Experimentally a size dependence is observed as the plasmon band is strongly damped for small particles and even disappears completely for nanoparticles less than about 2 nm (31a,b; 32). Very small nanoparticles in the size range below 2 nm are better treated as molecular clusters with discrete electronic states (see below), and the assumption of a delocalized free electron gas is no longer valid. But even for particles within an intermediate size range from 2–20 nm with established electronic bands, the question about the validity of bulk optical properties stemming from a bulk dielectric function arises. It has therefore been argued that the dielectric function needs to be modified to account for the smaller particle size before using Mie's equation in the dipole approximation. In one of the earliest attempts to account for the observed size effects, it was argued by Kreibig and coworkers (33a,b,c) in a classical picture that electron-surface scattering must be enhanced in small particles because the mean free path of the conduction electrons is limited by the physical dimensions of the nanoparticle. The mean free path of the electrons in silver and gold is on the order of 40–50 nm (30). Assuming that the dielectric function can be decomposed into a contribution from the interband transitions and a free electron part, the latter can be modified within the Drude free-electron model to account for enhanced electron-surface scattering as a function of the particle radius r. The dielectric function therefore becomes size dependent [$\varepsilon(\omega, r)$], and this can then explain the observed $1/r$ dependence of the plasmon bandwidth (17, 33). Because the material dielectric function itself is size dependent in contrast to the extrinsic size region (>20 nm), size effects for smaller nanoparticles are called intrinsic size effects (17).

This approach allows the calculation of absorption spectra over a wide range of sizes using the same equations first developed by Mie, which made this method of correcting for small particle-size effects so attractive. Many other effects like the "spill out" of the conduction electrons have also been considered and were incorporated by changing the bulk dielectric function appropriately (34–44). On the other hand, for small nanoparticles below 5 nm the direct computation of the polarizability of the nanoparticles can be accomplished by quantum mechanical calculation. The jellium approximation (42) for example neglects the structure of the ion lattice and replaces it by a uniform, positively charged background. The optical response is then calculated with the Time Dependent Local Density Approximation (TDLDA) using the density functional formalism. Palpant et al. (45a) prepared gold clusters in the 2–4 nm size range and found that the plasmon absorption is damped and blueshifted with decreasing particle size. The experimental results can be understood in the framework of the TDLDA, including the electronic density spill-out effect, the embedding matrix index, and the influence of d-electrons. A compilation and comprehensive overview of the different effects affecting the plasmon absorption band together with various theoretical approaches with references to the original work can be found in Reference 17.

Mie's theory was developed for particles of spherical shape only. For cylindrical or oblate nanoparticles, Gans (46) extended Mie's theory within the dipole approximation. The particles are usually characterized by their aspect ratio, which is defined by the ratio between the length and the width of the particle. The plasmon resonance for nanorods splits into two bands. As the aspect ratio increases, the energy separation between the resonance frequencies of the two plasmon bands increases (47–49). The high-energy band corresponds to the oscillation of the electrons perpendicular to the major rod axis and is referred to as the transverse plasmon absorption. The other absorption band, which is redshifted to lower energies, is caused by the oscillation of the electrons along the major rod axis and is known as the longitudinal surface plasmon absorption. Figure 2*a* shows the absorption spectrum of a nanorod sample having an aspect ratio of 3.3 compared to the 22-nm nanodots. The inset shows how the maxima of the transverse (squares) and longitudinal (spheres) surface plasmon modes vary with aspect ratio. The transverse plasmon absorption band is relatively insensitive to the nanorod aspect ratio and coincides spectrally with the surface plasmon oscillation of the nanodots. The linear spectral dependence of the longitudinal surface plasmon absorption can be reproduced using Gans' theory (48, 49).

Also shown in Figure 2*b* is the absorption of mixed gold-silver alloy nanoparticles with a gold mole fraction $x_{Au} = 0.27$. The plasmon absorption can be shifted linearly with the mole fraction between the maxima of pure silver (400 nm) and pure gold (520 nm) nanodots, allowing controlled tuning of the absorption band (50). In Figure 2*b* the experimental spectrum of the gold-silver alloy nanoparticles is compared to a calculated spectrum using the dipole approximation (Equation 1) and the dielectric function of the gold-silver alloy determined from a thin film

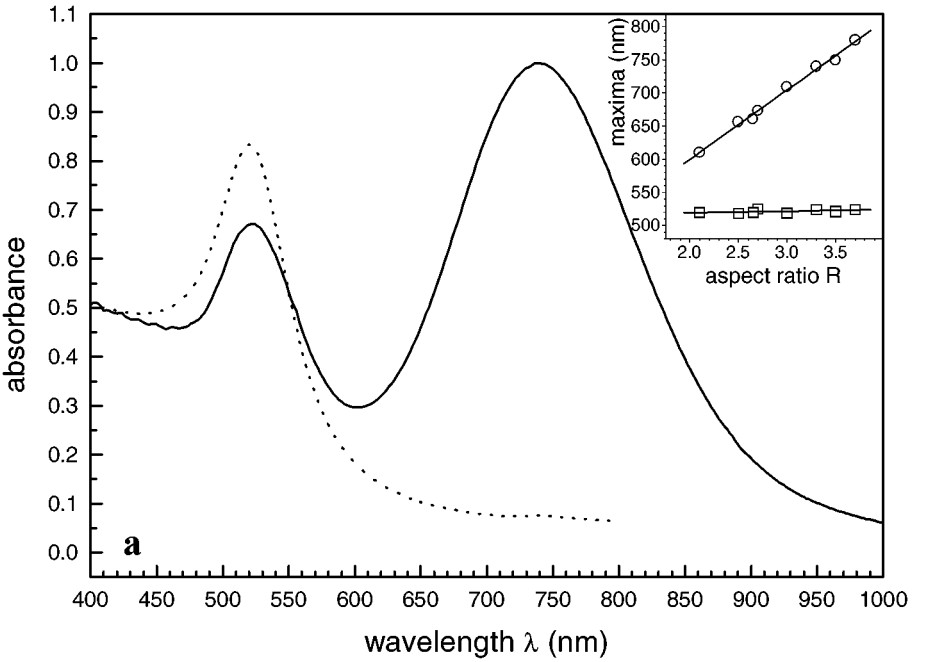

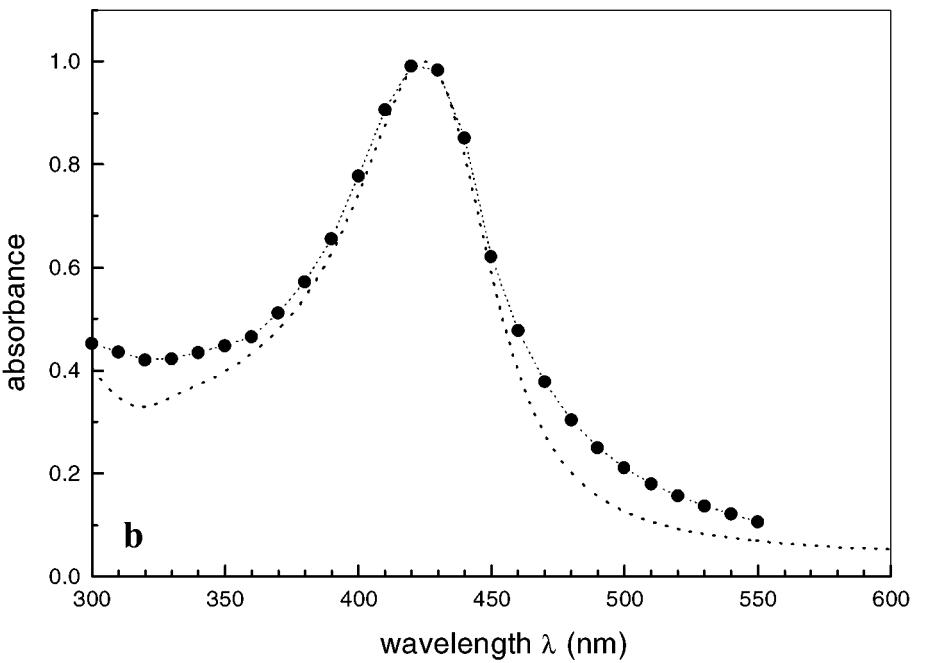

with a similar composition ($x_{Au} = 0.28$). This shows the good agreement and applicability of Mie's theory with experiment and also verifies the formation of alloy particles through the use of the dielectric function of the alloy.

In general, Mie's theory is only valid for very low concentrations of the nanoparticles in a solvent or solid matrix. It is assumed that the individual particles are noninteracting and separated far enough that the electric field created around one particle by the excitation of a surface plasmon resonance is not felt by other surrounding particles. If the interparticle distances become smaller than the spherical particle dimensions, or even when aggregation occurs, the plasmon resonance redshifts, and often a second absorption peak at longer wavelength is observed (17, 51). This second band could be regarded as a longitudinal resonance similar to the nanorods in case of chain-like aggregation of the individual nanodots. In the case of particle aggregation, and for composite materials like densely packed nanoparticles in a transparent host medium or nanoparticle assemblies (see below), effective medium theories are better suited to explain their optical absorption spectra (17–20).

Maxwell-Garnett theory (52), an effective medium theory, treats materials in which particles are isolated from each other by a layer of an insulating dielectric. However, particle dimensions and interparticle distances are considered to be infinitely small compared to the wavelength of the interacting light. Maxwell-Garnett theory is based on the Clausius-Masotti equation, and it assumes that it is justified to describe the composite material containing metal nanoparticles embedded in an inert host medium by an effective complex dielectric constant, which in turn is related to the optical refractive index and the absorption coefficient.

Martin and coworkers (53a–e) have used and extended Maxwell-Garnett theory in order to explain the optical absorption spectra of needle-like and pancake-like gold nanoparticles in a porous alumina membrane. The particles are prepared by electrochemical deposition of the gold into the nanopores of the template. The particles are all well aligned in one direction parallel to each other, and the aspect ratio can be controlled by the total deposition time.

It has become necessary, however, to account for the optical absorption properties and the shifts in the plasmon resonance for any arbitrary shape of the particles. Schatz (54) has developed and applied the finite element discrete dipole approximation (DDA) theory to nonspherical particles in particular nanoparticle arrays with varying size, shape, substrate, and solvent coverage produced by the nanosphere lithography (55) method pioneered by Van Duyne et al. (see below for more

←

Figure 2 (*a*) Absorption spectra of 22-nm gold nanodots (*dotted line*) and gold nanorods having an aspect ratio of 3.3 (*solid line*). The inset shows the dependence of the transverse (*squares*) and longitudinal (*circles*) plasmon absorption maxima on the aspect ratio. (*b*) Absorption spectrum of gold-silver alloy nanoparticles with a gold mole fraction of 0.27 (*dotted line*) and the calculated Mie spectrum.

details). DDA methods divide the particle into a large number of polarizable cubes, and their induced dipole polarizations are determined self consistently. From these polarizations the overall extinction cross section can be determined. DDA theory has also been recently applied to nanoprisms (56) produced by photoinduced irradiation of silver nanospheres and was able to reproduce the spectral shape of the nondegenerate plasmon resonances.

THE RELAXATION OF THE COHERENT PLASMON OSCILLATION

Although the plasmon absorption has been well understood in terms of the electromagnetic interaction between the metal particles and light, less is known about the decay mechanism of the coherent electron motion. Two decay mechanisms and times have to be considered here. The dephasing of the electron motion leads to the loss of the coherence. The speed of the dephasing is typically characterized by the time constant T_2, which is related to the inelastic decay time of the plasmon absorption (energy decay) T_1 and the pure elastic dephasing time T_2^* by (57):

$$\frac{1}{T_2} = \frac{\Gamma}{2 \cdot h} = \frac{1}{2 \cdot T_1} + \frac{1}{T_2^*}, \qquad 2.$$

where Γ is the homogeneous spectral linewidth. T_2^*, the pure dephasing time, may originate from collisions that change the plasmon wave vector but not its energy. Often T_2^* is much shorter than the energy relaxation T_1 and decreases rapidly with temperature. It then determines the value of T_2. However, it is an open question how and if T_2^* contributes at all (58). Relaxation pathways for the plasmon energy decay T_1 include the radiative decay of the plasmon, which accounts for only a small contribution [1.5% for a 20-nm particle (17)] and the nonradiative decay into single electron-hole excitations. Depending on the location of the hole within the conduction band or in the lower-lying bands, this can lead to intraband or interband excitation, respectively. This would depend on the energetic overlap of the plasmon resonance with the energy threshold of the interband transitions. Lehmann et al. (59a,b) have shown experimentally by femtosecond time-resolved two-photon photoemission from silver clusters supported on graphite that the resonant plasmon excitation by two photons leads to either a single photoelectron or to the creation of at least two single-particle excitations, which share the total energy, thus confirming the decay of a plasmon resonance into a single electron-hole excitation.

Assuming a homogeneous size distribution and therefore homogeneous line broadening, the total dephasing time can be computed from the measured width of the plasmon bands using Equation 2. For the plasmon absorption of the 22-nm nanodots in Figure 2*a*, this would give a dephasing time of about 4 fs (60). Using nonlinear frequency mixing studies, instead of the simple spectral linewidth

analysis, Heilweil et al. (57) found that both T_1 and T_2 are shorter than 48 fs for colloidal gold nanoparticle solutions. Lamprecht et al. (61a,b) measured T_2 for lithographically produced 200-nm gold and silver nanoparticles by a second-order nonlinear optical autocorrelation method in the femtosecond regime. They obtained dephasing times of 6 and 7 fs for gold and silver, respectively. The lithographically prepared particles were much larger than the particles used in the examples given above (which were about 20 nm in diameter) but had the advantage of being very regular in size and shape.

A narrow size and shape distribution of the nanoparticles is essential for determining T_2 accurately. Liau et al. (62) therefore combined a two-pulse second-order interferometric autocorrelation method with an optical microscope, which allowed them to measure the response from single silver nanoparticles with a size of 75 nm. The setup further included an atomic force microscope (AFM) for correlated structure-function analysis. They determined a dephasing time T_2 of 10 fs.

Klar et al. (63) measured the near-field transmission spectra of individual gold nanoparticles with an average size of 40 nm using a scanning near-field optical microscope (SNOM) and obtained dephasing times extracted from the homogeneous linewidth varying around 8 fs. Deviations of individual particles from this value were attributed to variations in the local environment. Furthermore, some particles showed broad resonances with two maxima, which were attributed to interparticle coupling. Whereas the last two examples showed the capability of single-particle studies, a much simpler approach is to use a conventional microscope and illumination with a halogen lamp, taking advantage of the large scattering cross sections of metal nanoparticles. This approach was chosen by Itoh et al. (64). They embedded 40-nm gold nanoparticles in PVA film of varying thickness and found a strong dependence of the plasmon resonance frequency on the environment of the particles as the plasmon absorption redshifts with increasing film thickness. In the thinner films the particles were assumed to be partially surrounded by air, which accounts for the change in the local environment.

Single particle studies seem to be ideally suited to measure the homogeneous linewidth, and hence T_2, without the problems associated with an inhomogenous size distribution. With the simple setup of an optical microscope the homogeneous linewidth was measured for gold nanodots and nanorods by Soennichsen et al. (58, 65). They found much longer dephasing times for gold nanorods of up to 18 fs determined from the homogeneous width of the longitudinal surface plasmon resonance compared to 1–5 fs for nanodots, and they explained their results with a reduced interband damping in the nanorods because of a decreased spectral overlap between the longitudinal plasmon resonance at lower energies and the interband transition. They furthermore concluded that pure dephasing T_2^* is negligible and the plasmon dephasing T_2 is mainly dominated by nonradiative decay T_1 into single-particle excitation.

The single-particle studies discussed above raise the question of whether the frequency shift of the plasmon resonance as well as the variation in the plasmon

bandwidth related to T_2 can simply be accounted for by the dielectric constant of the surrounding medium as predicted by the Mie equation in the dipole approximation (Equation 1). In an elegant study by Kreibig et al. (66a,b), dephasing times of 2 and 7 fs for 2-nm silver clusters embedded in a matrix and in vacuum (naked clusters) were determined from the width of the plasmon band. To account for this large difference they explained the experimental results using a model known as chemical interface damping (44), in which the empty LUMO orbitals of the acceptor molecules on the particle surface can couple with the free electrons in the conduction band of the metal. The smaller the energy difference is between the donor and acceptor levels, the stronger the coupling is. Electron transfer between the levels becomes possible after excitation of a plasmon resonance. After the excited electrons have transferred into the empty acceptor levels and then back, they have lost coherence with the rest of the electrons excited during the plasmon excitation. This in turn then corresponds to a broader bandwidth because of a faster dephasing. As the electronic structure and therefore the energetic position of the LUMO varies for different adsorbate molecules, it is expected that the plasmon resonance of the same metal cluster will experience different degrees of damping depending on the specific electronic structure of the surface-bound molecules relative to those of the metallic electronic structure (Fermi level) and not just depending on the effective dielectric constant of the medium. Indeed, this is what Kreibig et al. (66) found experimentally when the same silver clusters produced in the gas phase are first deposited on a SiO_2 substrate and then later embedded in SiO_2 by co-deposition of SiO_2. Single particle studies with metal nanoparticles embedded in different media might be able to shed further light on the influence of the chemical nature of the interface.

Spectral hole burning is another technique that gives information about the homogeneous linewidth of an absorption, which was recently applied to small supported oblate silver nanoparticles with radii of 7.5 nm (67a,b). Stietz et al. took advantage of the shape dependence of the plasmon resonance for the oblate particles and the possibility of inducing a shape change by laser irradiation with a narrow linewidth nanosecond laser. Laser irradiation leads to a shape change of the oblate particles by atom evaporation causing a transformation to more spherical particles. This in turn results in a decrease of the plasmon intensity for the particles with a certain aspect ratio absorbing at the frequency of the laser (see also below the discussion on the laser-induced shape changes of metal nanoparticles). The difference spectrum between before and after laser irradiation gives an optical hole whose linewidth is assumed to be homogeneously broadened when extrapolated to low laser fluences. A dephasing time of 4.8 fs was extracted by this method for the silver particles with a mean radius of 7.5 nm.

The knowledge of T_2 is not only important for the basic understanding of the decay mechanisms of the plasmon resonance, but also T_2 is furthermore related to the enhancement factor of the electric field near the particle surface (17). This local field enhancement is important in applications such as SERS and plays a

crucial role for the observation of luminescence from metallic nanoparticles. Both phenomena are discussed next.

ENHANCED LUMINESCENCE PROPERTIES OF METAL NANOPARTICLES

Photoluminescence from bulk copper and gold was first observed by Mooradian (68) and has been used extensively in characterizing the carrier relaxation and the band structure of metals (69–74). It was found that the emission peak was centered near the interband absorption edge of the metal and therefore was attributed to direct radiative recombination of the excited electrons with holes in the d-band. However, the quantum efficiency of the photoluminescence from bulk noble metals is very low, typically on the order of 10^{-10} (68). A more extensive experimental study on the photoluminescence of copper, silver, and gold was carried out by Boyd et al. (70). They were able to model their experimental results and determined the relation between the spectral peaks and the interband recombinations at selected symmetry points in the Brillouin zone. Furthermore, Boyd et al. (70) also studied the effect of the surface roughness on the photoluminescence properties of noble metals. Surprisingly, the luminescence is enhanced by several orders of magnitude on rough metal surfaces, which is known as the lightning rod effect (70; 75a,b). Roughing metal surfaces can be thought of as creating a collection of randomly oriented hemispheroids of nanometer dimensions on the smooth surfaces. These hemispheroids show a surface plasmon resonance similar to the gold nanorods, and therefore the incoming and outgoing electric fields are amplified by the local field created around the hemispheroids by the plasmon resonances.

This kind of enhancement has been proposed for the observed luminescence of gold nanorods (76). The luminescence efficiency is found to increase by six orders of magnitude because of this lightning rod effect. Figure 3*a* and 3*b* show the absorption and steady-state fluorescence spectra, respectively, of three gold nanorod samples having average aspect ratios of 2.6, 3.3, and 5.4. The spectra reveal the presence of an emission band between 550 and 600 nm. The fluorescence maximum redshifts with increasing nanorod aspect ratio. This is illustrated in the inset of Figure 3*b*, where the fluorescence maximum is plotted against the nanorod aspect ratio. A linear dependence is found experimentally (76). Furthermore, the luminescence quantum efficiency increases linearly with the square of the aspect ratio (76). On the other hand, gold nanodots with diameters between 20 and 30 nm prepared by the same electrochemical method do not show a comparable emission. This leads to the conclusion that the longitudinal plasmon resonance absorbing at longer wavelengths is more effective in amplifying the fluorescence in gold nanoparticles compared to the surface plasmon resonance of spheres as the longitudinal plasmon resonance is less damped. This is in agreement with the longer dephasing times measured for the rods (58).

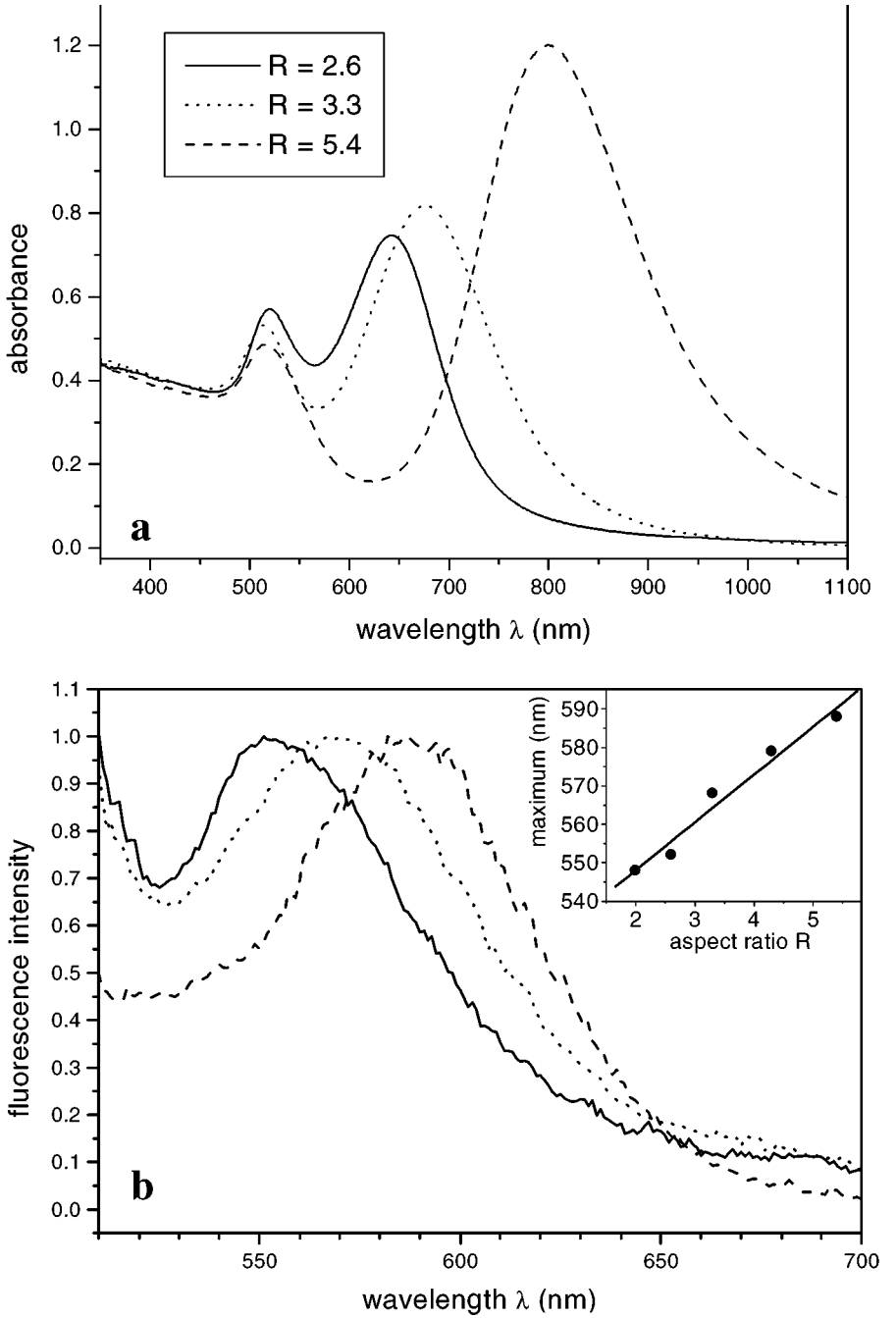

Figure 3 Absorption (*a*) and luminescence (*b*) spectra of colloidal gold nanorods with aspect ratios of 2.6, 3.3, and 5.4 (480-nm excitation). The inset shows the linear dependence of the luminescence maximum on the aspect ratio.

Wilcoxon et al. (77) reported that very small spherical gold clusters (<5 nm) show an emission at 440 nm when excited at 230 nm. The quantum yield is increased to 10^{-4}–10^{-5} compared to the value of bulk gold, similar to the enhancement of the photoluminescence of gold nanorods. The same authors also found that the luminescence is absent in larger nanodots of 15 nm in diameter. They furthermore observed a difference in the photoluminescence for particles prepared in water compared to particles prepared in an oil-based inverse micelle method, where the latter shows an additional redshifted luminescence peak.

In both studies, the origin of the photoluminescence was attributed to the radiative recombination of an electron-hole pair. The incident photons are initially absorbed by the d-band electrons leading to interband transitions. The photon energy promotes these electrons from the filled d-band to electronic states above the Fermi level in the sp-conduction band. Both electrons and holes can relax by scattering with phonons but then recombine radiatively to give rise to the observed luminescence. Such an intrinsic emission profile is then modified by the local field created around the nanoparticles caused by excitation of the plasmon resonance. The theory of the local field effect has been successfully applied in various cases to explain results on second harmonic generation, surface-enhanced Raman scattering, and luminescence observed from rough noble metal surfaces (70; 75a,b). The same theory was also applied to the luminescence of gold nanorods and was able to reproduce the linear dependence of the luminescence maximum and the quadratic dependence of the quantum yield on the aspect ratio (76).

Using time-resolved femtosecond fluorescence up-conversion Varnavski et al. (78) studied the ultrafast photoluminescence dynamics of gold- and silver-dendrimer nanocomposites with a metal size of about 15 nm. They found a fast 70 fs fluorescence decay component associated with the luminescence from the metal core and attributed its increased magnitude to the local field enhancement. Anisotropy measurements show that the luminescence is depolarized, which agrees well with an even faster dephasing time as discussed above.

ENHANCED SURFACE RAMAN SCATTERING OF MOLECULES ON NANOCRYSTALS

The same local field effect is also observed in Raman scattering from molecules absorbed on the surfaces of rough metals, nanoparticle aggregates, or single nanoparticles (71, 79–90). The surface enhanced Raman Scattering (SERS) signal is enhanced by several orders of magnitude. Typical enhancement factors for ensemble measurements are about 10^6–10^7 (71, 79–81), which are attributed to the enhancement of the otherwise weak Raman scattering signal by the electromagnetic field near the particle's surface. Particularly high enhancement seems to exist for aggregated colloidal silver or gold nanoparticles induced by halide ions (71, 81, 83). Plasmon resonances in such structures can result in a strong confinement of the optical field in very small areas between the aggregated particles (hot spots). The exact role of the halide ions, beyond inducing the particle aggregation, is

however not clear. A second enhancement mechanism, which contributes to the SERS, is the chemical interaction of the surface-adsorbed molecule with the metal. Chemisorbed molecules experience an additional enhancement of about 10^2 compared to physisorbed particles (71, 79–81), which may result from a resonant scattering process caused by an absorption-induced metal-to-molecule or molecule-to-metal charge transfer electronic transition. The nanoparticles can therefore be regarded as nanoamplifiers, and since the discovery of this effect, SERS has been studied intensively (71, 79–90). It is a convenient tool of increasing the sensitivity of the otherwise weak Raman signal.

The role of the nanoparticle shape on the SERS enhancement was studied by Nikoobakht et al. (89a) who found that gold nanorods showed a significant SERS effect for the adsorbed surfactant molecules whereas nanodots showed no activity under similar conditions in which the nanoparticles were adsorbed on silicon or alumina substrates. Pyridine also showed an enhanced Raman signal when adsorbed to the nanorods. The excitation wavelength was 1064 nm, which is close to the longitudinal plasmon resonance compared to the spheres but not in direct resonance. The ability to tune the plasmon resonance to the wavelength of the excitation light by changing the aspect ratio of the nanorods is demonstrated by the same workers (B. Nikoobakht, M.A. El-Sayed, unpublished manuscript). Similarly, gold and silver nanoshell particles have been tailored by Halas and coworkers (90) so that their plasmon absorption becomes resonant with the Raman excitation wavelength in the IR. They have found optimum SERS intensities when enough gold is deposited on the silica cores to form a nearly complete metal shell. Further metal deposition leads to a decrease in the SERS intensity.

Because of the large enhancement factor observed for SERS, single-particle studies have recently been carried out by several groups investigating the SERS signal from molecules on a single nanoparticle (85–88). Interestingly, some very different results compared to the ensemble measurements have been found. The most important observations, which have come about from these experiments, are that not all metal nanoparticle surfaces are SERS active and that the single particle enhancement factor is actually on the order of 10^{14}–10^{15} (85a–d; 86). This fact was completely missed by ensemble measurement, although the existence of "hot" particles has been suggested (83) owing to the nonlinear increase of the SERS intensity with the analyte molecule concentration.

Nie and coworkers (85a–d) studied the SERS of rhodamine 6G on silver particles. Combining an optical microscope with an AFM, they carried out structural studies on the same SERS active silver particles and found that for longer excitation wavelengths the SERS active particles have a larger diameter. The distribution of active particles for a certain wavelength falls into a rather narrow size range. Similar results were obtained for gold nanoparticles, and they showed that 60–70-nm particles are most active at 647-nm laser excitation. Aggregation of particles furthermore revealed an increased SERS intensity but does not produce optically "hot" aggregates if the individual particles are not active themselves. Activation can however occur through addition of halide ions. A complex formed on the particle surface between a metal cation, a halide anion, and the analyte molecule is

suggested to be the active site for SERS. Performing time-resolved studies, the same authors also observed an intermittent light emission, which is a clear feature of single-particle spectroscopy. It is usually attributed to molecular oxygen quenching of the fluorescence, although its origin in SERS is less understood. Possible explanations (85c) involve photoinduced ionization and thermally activated diffusion of the molecule on the particle surface.

Kneipp et al. (86) independently developed single-particle SERS using crystal violet adsorbed on silver nanoparticles and near infrared excitation, which allowed for nonresonant excitation conditions. Under nonresonant conditions they also observed an enhancement factor of 10^{14}. They further demonstrated that single particle SERS can be extended to surface-enhanced hyper-Raman scattering as well as surface-enhanced anti-Stokes Raman scattering as tools for nonlinear single-molecule Raman spectroscopy. For the normally weak surface-enhanced hyper-Raman scattering, an enhancement factor of 10^{20} was obtained.

Michaels et al. (87a,b) and also Xu et al. (88) show by AFM and optical imaging that the silver nanoparticles, which yield SERS of single molecules, are all compact aggregates of at least two individual particles. The adsorbed molecules are most likely located at the junction between two particles. Michaels et al. (87a,b) further showed that there is no direct correlation between the Rayleigh scattering from the active metal nanoparticles and the SERS intensity. The Rayleigh scattering spectrum shows the plasmon absorption of the metal nanoparticle, which can vary greatly for different sizes and shapes. The authors argue that factors other than simply an intense plasmon resonance are responsible for the observed large enhancement factors for single-molecule SERS.

Although more work seems to be necessary to distinguish and clarify the different enhancement mechanism and to find the optimum particle size and shape and activation, it can already be concluded that single-particle SERS provides a powerful tool to investigate single molecules absorbed to the nanoparticle surface. The metal particles in this case only serve as amplifiers of the Raman signal whereas the adsorbed molecules can be studied through their Raman spectrum. The overall advantage of single-particle SERS compared to single-molecule fluorescence is that Raman spectroscopy actually yields molecular structure information. Furthermore, the duty cycle of the molecule in SERS is high because of the lack of direct electronic excitation, which leads to molecule bleaching in fluorescence microscopy. Furthermore, this opens the possibility of studying biomolecules, which usually have a very low fluorescence quantum yield.

ULTRAFAST DYNAMICS: ELECTRON-PHONON AND PHONON-PHONON RELAXATION IN NANOCRYSTALS

The interaction between metal nanoparticles with femtosecond laser light has been of great interest recently (91–103) as time-resolved transient absorption spectroscopy allows one to follow the electron relaxation dynamics. The excitation of the electrons by a femtosecond laser pulse leads to a perturbation of the electron

distribution in the metal, which is given by a Fermi distribution. The initially created electron distribution is highly nonthermal, and the first relaxation step is the electron thermalization by electron-electron scattering establishing a new Fermi electron distribution corresponding to a higher temperature. This is extremely fast in bulk metals [500 fs for gold (104) and 350 fs for silver (105)], and Vallee and coworkers have studied the size dependence of this first relaxation step for silver nanoparticles with radii between 1.6 to 13 nm embedded in glass matrices under low excitation powers (106). The electron thermalization manifests itself in a slower rise time of the transient signal compared to the 60-fs probe pulses. They found an increase in the electron energy exchange rate for nanoparticles smaller than 5 nm, which they attribute to enhanced electron-electron scattering caused by surface-induced reduction of the Coulomb interaction screening by the conduction and core electrons and possible electron-surface scattering.

The electron thermalization is followed by the energy exchange between the electrons and the lattice via electron-phonon coupling. The electron-phonon coupling was found to be size and shape independent for gold nanoparticles in the size range from 2 to 120 nm and rods of aspect ratio from 2 to 5 (95; 96a,b). The measured electron-phonon relaxation times depend on the laser pump power and are on the order of a few picoseconds (1–4 ps). The results obtained for the nanoparticles, furthermore, compare well with the electron-phonon coupling constant measured for bulk metal using similar time-resolved laser techniques (104).

The independence of the electron-phonon relaxation in gold nanoparticles is rather surprising considering that the mean free path of the electrons is only about 40 nm. In particles smaller than 40 nm, electron-surface scattering should become more frequent than electron-lattice scattering itself. Therefore it was thought that enhanced electron-surface coupling in small particles should give rise to a pronounced size dependence for the electron cooling dynamics in particles smaller than the electron mean free path. Indeed this is thought to be the reason for the increased dephasing times of the coherent plasmon oscillation in small particles leading to a broader plasmon absorption band as discussed above. However, for the electron-phonon relaxation dynamics this is not observed experimentally. Using a theory developed by Belotskii et al. (107), Hartland and coworkers (108) showed that the coupling constant between the electrons with acoustic and capillary modes of the surface phonons is determined by the ratio of the number of valence electrons in the atom to the atomic mass of the metal. Because of the small number of the valence electrons in gold (only one electron) combined with a large atomic mass, the contribution of electron-surface scattering to the overall electron-phonon scattering cross section is very small. Hartland et al. have calculated a contribution of less than 10%. Consistent with this model are also the results obtained by Stella et al. (109) who reported a size-dependent electron–surface interaction for 2-, 4-, and 6-nm tin particles embedded in an Al_2O_3 matrix by femtosecond transient reflectivity measurements. They measured decreasing lifetimes with decreasing size corresponding to an increase in electron-surface scattering in the tin nanoparticles where the mean free path is 4.4 nm. In comparison to gold, tin is a much lighter

element with 4 valence electrons, and the experimentally observed size effect is in agreement with this model.

The pump power dependence of the electron-phonon relaxation is explained by the temperature dependence of the electronic heat capacity leading to longer relaxation times at high pump intensities (95; 96a,b). In the low perturbation regime, using very weak laser excitation, the electron-phonon relaxation actually becomes pump power independent. Under these conditions, Del Fatti et al. (110) reported a decrease in the electron-phonon relaxation times from 800 to 500 fs for silver nanoparticles in a glass matrix as the size is reduced from 30 nm to 4 nm with a change of relaxation times occurring for particles smaller than 10 nm in diameter. They attributed the size dependence of the electron-phonon relaxation to an enhanced inelastic electron-surface scattering. The difference in the size dependence of the electron-phonon relaxation time observed for the silver particles compared to the gold nanoparticles discussed above might be explained by the fact that the experiments on gold were mainly performed under strong excitation conditions and extrapolated to the low power regime. The possibility of a contribution from the surrounding matrix might also be considered.

Experimentally, the described processes manifest themselves in a bleaching of the plasmon band in the case of gold nanoparticles. Figure 4 shows the transient absorption spectra of 15-nm spherical gold nanoparticles excited at 400 nm with femtosecond pulses and probed at different delay times. The inset shows the decay of the bleach intensity at the plasmon maximum from which the electron-phonon relaxation can be determined. Physically, this transient behavior of the plasmon band bleaching can also be understood as a faster dephasing time T_2 of the coherent plasmon oscillation as argued by Perner et al. (94). At higher temperatures the occupation of higher electronic states leads to an increased electron-scattering rate as known from Fermi liquid theory (30) and thus to an increased damping of the plasmon oscillation. Perner et al. found an increase of the plasmon bandwidth of gold nanoparticles embedded in a sol-gel matrix by 120 meV and calculated an average electron-electron-scattering rate of $(10\ \text{fs})^{-1}$ for a hot electron distribution at 4000 K. Hartland and coworkers (95) on the other hand, argue that the plasmon band bleach in gold nanoparticles can be fully explained by a modification of the dielectric function as a result of an increased electron temperature. This modified dielectric function then enters through the Mie equation by which the plasmon band absorption can be calculated for a higher electron temperature. The observed spectra are the difference spectra between the ground state absorption and the plasmon absorption at an elevated temperature. Vallee and coworkers (91) have performed extensive calculations in combination with their experiments, exclusively performed in the low perturbation regime, in order to analyze the contribution of the core and conduction electrons, respectively, to the observed transient signal in mainly silver and also gold nanoparticles. They also use the approach of a temperature-modified dielectric constant in analogy to their prior work on thin metallic films (104). Although the exact physical origin of the observed transient absorption signal might be debated in the literature there is no argument that the

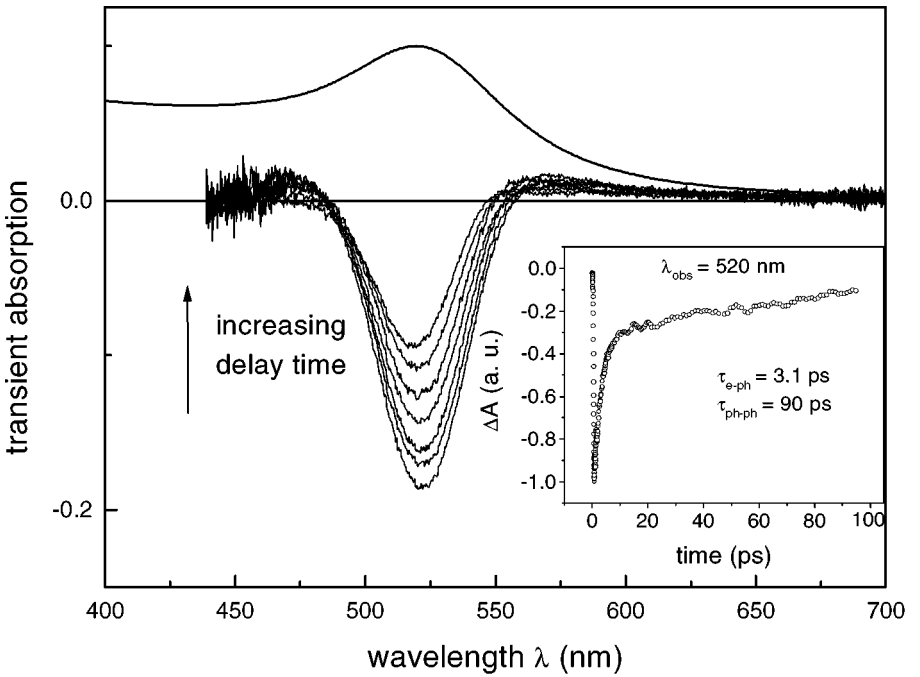

Figure 4 Transient absorption spectra of 15-nm gold nanodots recorded at various delay times after excitation with 400-nm femtosecond laser pulses together with the ground state absorption. The inset shows the recovery of the transient absorption signal monitored at the plasmon bleach maximum (520 nm).

plasmon resonance is a useful and very sensitive probe for the electron dynamics in confined metallic systems.

The recovery of the bleach is related not only to the energy exchange between the excited electrons and the particle lattice, but also between the particle and its surrounding medium by phonon-phonon coupling. This last step can be correlated to the long decay time observed in the transient absorption dynamics as seen in the inset of Figure 4. The phonon-phonon coupling is on the order of several hundred picoseconds as measured for metallic nanoparticles in solution as well as in a glass matrix (94–96a,b). The phonon-phonon relaxation time is proportional to the square of the particle radius as recently shown by Hu et al. (111) for gold nanoparticles in aqueous solution.

The effect of changing the surrounding medium was studied by El-Sayed and coworkers (112a,b) who found that the surrounding medium has a significant effect on the cooling dynamics of the hot electrons in gold nanoparticles. Both of the two decay components of the plasmon bleach recovery (electron-phonon and phonon-phonon) are influenced by the surrounding medium when the medium is changed from an organic solution to $MgSO_4$ powder (112a) or from aqueous solution to a

series of polymer gels (hydrogel and different organic gels) (112b). The recovery times become slower when the thermal contact between the particles and the matrix is decreased (as in the $MgSO_4$ powder system) or when the thermal conductivity of the medium is decreased (as for the organic gels compared to the hydrogel). These results confirm that the surface properties of the metallic nanoparticles and the thermal properties of the surrounding medium play important roles in the cooling dynamics of the hot carriers in metallic nanoparticles. Similar results have been obtained by Bigot et al. (113) who measured the relaxation dynamics of 6.5-nm silver nanoparticles embedded in two different types of transparent glasses (alumina and glass). They found an increase of the electron-phonon relaxation time from 0.77 to 1.4 ps when comparing the alumina and glass matrices, respectively. They explained their results in terms of the better heat conductivity of the alumina. An interesting study was also recently reported by Westcott et al. (114) who showed that the chemical nature of surface-adsorbed molecules could have an effect on the electron dynamics of gold core-shell nanoparticles. They found that the molecules providing the strongest change in the dynamics decreasing the electron relaxation time from 2.7 ps to 1.7 ps have the largest induced dipole moments near the metal surface. More experiments are necessary to elucidate the mechanism involved in the heat transfer from the gold nanoparticles to the surrounding matrix (i.e., the nature of the particle-maxtrix coupling and the type of phonons involved) and the heat transport away from the hot particles.

ACOUSTIC BREATHING MODES OF NANOCRYSTALS

For spherical particles, an acoustic breathing of the hot nanoparticles has been observed in the femtosecond pump-probe studies (115–118a,b). Because of the fast heating of the electrons and the lattice with a femtosecond laser pulse, the increase of the lattice temperature causes the particles to expand. If the timescale for heating is faster than the period of an acoustic phonon mode of the nanoparticle, then this mode can be excited impulsively. This coherent volume change of the nanoparticles (breathing) can be observed experimentally by femtosecond transient absorption spectroscopy because a volume change of the particles causes a shift in the plasmon absorption maximum. At the high energy side of the plasmon band the acoustic breathing causes an oscillation of the transient absorption, which is 180 degrees out of phase with respect to the signal observed at the low energy side. These breathing modes can be accurately modeled by a damped harmonic oscillator with the thermal lattice expansion caused by laser heating as the driving force (115a–d; 116). Good agreement between theory and experiment is found when the pressure caused by the hot electron gas produced during laser excitation is taken into account in order to reproduce the correct initial phase of the oscillations (115a–d). It was further found that the frequencies of the acoustic modes are inversely proportional to the nanoparticle radius (115a–d; 116), and for silver nanorods (117) two oscillation periods were observed for the transverse and longitudinal mode, respectively. Gold nanorods were investigated as well (115d), and it was found that the oscillation

period depends linearly on the nanorod length. Because of the size polydispersity of the gold nanorod samples, the measured period also depends on the observation wavelength.

A comparison between the oscillation frequency and damping rate for metallic particles in different media showed that the frequency is environment independent, while the damping rate is strongly influenced by the nature and acoustic response of the surrounding material (116). In a "soft" environment like the colloidal solutions, the damping is not influenced by particle-environment interactions, and the damping rate is determined by the inhomogenous size distribution of the sample, which in turn presents a way to measure the sample size distribution (115a–d). In a "hard" environment like a transparent glass matrix the coupling to the medium will determine the damping rate. The damping rate is therefore connected to the particle-environment interactions. On the other hand, the oscillation frequency is only dependent on the metal itself and can be related to the mechanical properties of the metal (through the Young's modulus, which enters the theoretical calculation of the spherical breathing modes). These types of investigations hence offer a great deal of information about the overall nanoparticle system, and optical techniques might be able to measure mechanical properties of nanoparticles otherwise inaccessible.

TRANSITION BETWEEN COLLECTIVE ELECTRONIC PROPERTIES AND THE MOLECULAR CLUSTER LIMIT

The metallic nanoparticles discussed so far all have a strong plasmon resonance dominating their optical properties. As mentioned above, the plasmon band in gold nanoparticles is strongly damped for smaller particles until it disappears for particles smaller than about 2 nm in size. The two-phase reduction method for the preparation of alkylthiol monolayer-protected gold particles first introduced by Schiffrin and coworkers (119) and used extensively by the groups of Whetten (31a,b) and Murray (32) has made it possible to study this small cluster regime in more detail without the use of a high-vacuum cluster-beam apparatus. The protected gold particles are stable and can be separated by chemical techniques for mass-spectroscopic analysis (32). Certain sizes have been found to be extremely stable in accordance with a magic number model. This class of particles allows the study of size-dependent properties especially in the limit of the particle-to-molecule transition regime. The former is dominated by collective electron behavior (plasmon resonance), whereas the latter shows single-electron excitation as well as chemical redox behavior as recently found by electrochemical measurements (120). Indeed, it was found that for particles studied in the size range between 1.1 and 1.9 nm, larger cores display Coulomb staircase responses consistent with double-layer charging of metal-electrolyte interfaces, while smaller cores exhibit redox chemical character, including a large central gap.

Among the smallest clusters synthesized is a very stable, water-soluble 28-atom gold cluster (121), which is capped by a monolayer of 16 tripeptide glutathione

units (GSH = γ-Glu-Cys-Gly). The optical absorption spectrum (see Figures 5*a*,*b*) of these clusters is well structured with a distinct absorption onset near 1.31 eV (950 nm) corresponding to the above mentioned electronic gap between the highest occupied (molecular) orbital and the lowest unoccupied orbital (HOMO-LUMO gap). A first strong absorption maximum is seen at 1.84 eV (675 nm) followed by a continuous increase in the absorption intensity at higher energies. Luminescence experiments (122) (see Figure 5*b*) found that these clusters have two separate luminescence bands with maxima at 1.5 and 1.15 eV (800 and 1100 nm). The total quantum yield of the luminescence as measured at ambient temperature is approximated to be about $3.5 \pm 1.0 * 10^{-3}$ with a lifetime in the microsecond range. Because of the unusually high luminescence quantum yield for a metallic cluster, it was suggested that the short- and long-wavelength luminescence bands could be assigned to the fluorescence and phosphorescence from excited singlet and triplet states, respectively, in analogy to the photophysical properties of a molecule (122). Femtosecond transient absorption studies (123) (see Figure 5*a*) further showed an induced transient absorption instead of a plasmon band bleach with a double-exponential decay that is independent of the laser pump power. These observations, especially when compared to the larger nanoparticles, clearly indicate a molecular-type behavior with single-electron excitation. Such a small cluster, with only 28 core atoms and a much bulkier organic ligand shell, should therefore be regarded as a molecule. In this example, nanoparticle research is closing the gap with the inorganic cluster field.

A similar small gold cluster stabilized by phosphine ligands has been the center of much attention. It is the Au_{55} cluster prepared in Schmid's group (124). It has mainly been investigated with respect to its structural characterization, but Smith et al. (125) also carried out femtosecond dynamics studies and came to a similar conclusion that this cluster should be treated more like a molecule when compared to larger particles.

The changes in electronic properties and the transition from a metal to a nonmetal have also very significant consequences for the chemical reactivity of the clusters. It should be mentioned that gold showed catalytic activity for the oxidation of CO with a maximum for 3.5-nm particles supported on titania (126). This is so surprising because bulk gold derives its noble character from its chemical inertness. One of the many examples why "small is different."

LASER PHOTOTHERMAL-INDUCED SHAPE CHANGES OF METAL NANOPARTICLES

Using laser light as a source of thermal energy provides the possibility of selectively heating the metallic nanoparticles inside a host medium while the surrounding material initially remains cold. This provides the opportunity to thermally change the size and shape of metallic nanoparticles through melting and evaporation at high-enough laser intensities (127–133a,b). For nonspherical particles the nondegenerate plasmon absorption allows one to selectively photothermally heat

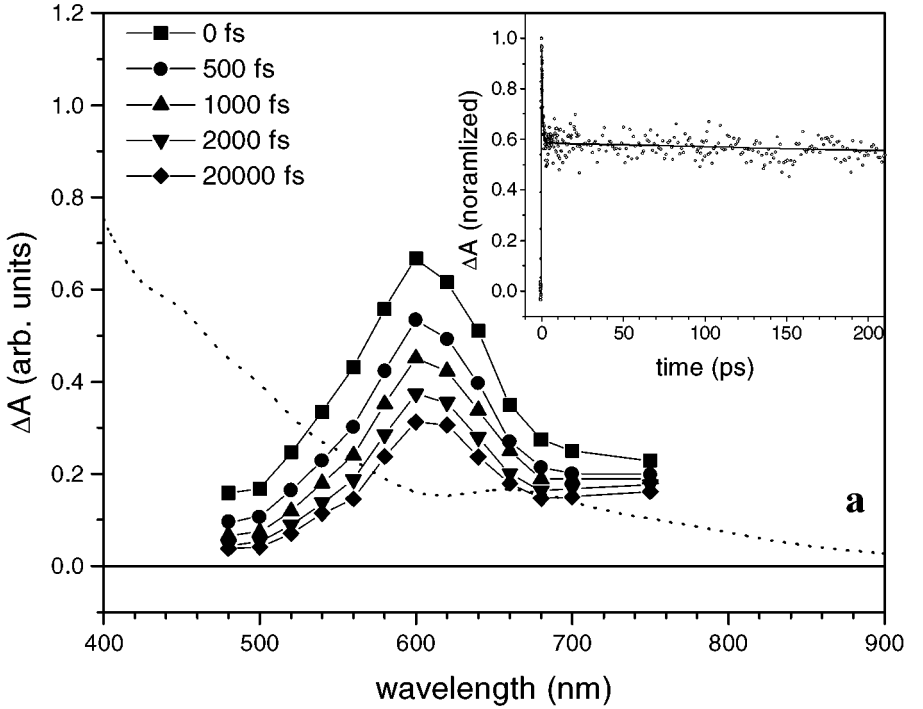

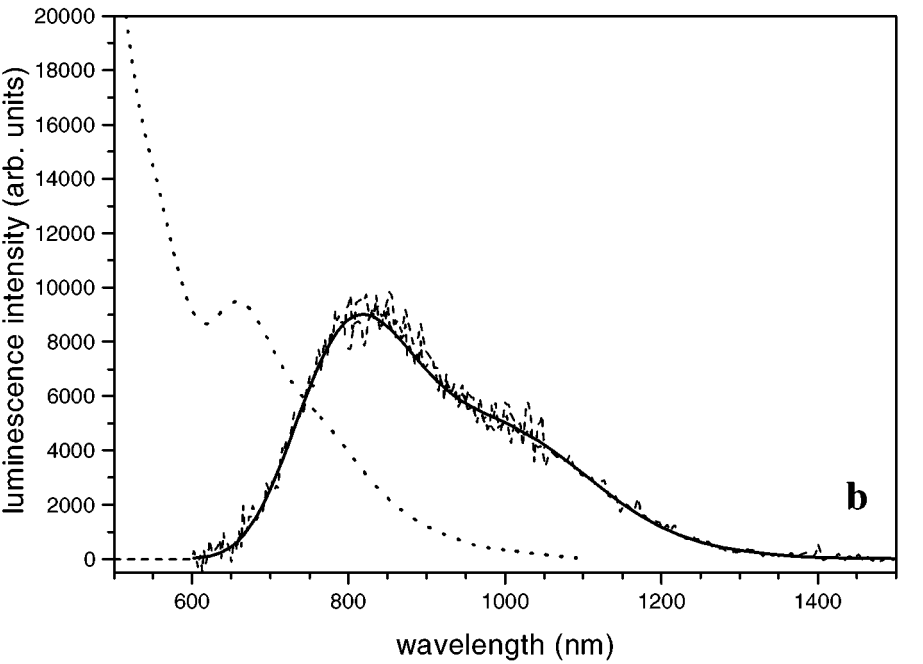

and thus change only a certain shape (aspect ratio) of a sample having a broad size and shape distribution (130–133a,b).

In the case of spherical nanoparticles, it has been reported that irradiation of gold particles with 532-nm nanosecond laser pulses leads to fragmentation of the nanodots as studied by Koda et al. (127a,b). This was explained in terms of the slow heat release of the deposited laser energy into the surrounding solvent, which leads to melting and even vaporization of the nanoparticles as estimated from the deposited laser energy and the absorption cross section. As the nanoparticles cannot cool off as fast as they are heated, they fragment into smaller nanodots. The size reduction of silver nanoparticles in a glass matrix induced by excimer laser irradiation at 248 nm was also explained by a thermal model (128). On the other hand, in a study on silver nanoparticles, which were irradiated with 355-nm picosecond laser pulses, Kamat et al. (129) proposed that the initial ejection of photoelectrons causes the particles to become positively charged. The repulsion between the charges then leads to fragmentation.

Although the above mentioned studies produced smaller particles from a starting distribution of spherical nanoparticles mainly by fragmentation, Bosbach et al. (132a,b) took advantage of the fact that nonspherical particles can be irradiated selectively depending on their shape as the laser frequency can be tuned to a certain narrow frequency of the surface plasmon resonance corresponding to a certain shape. In this manner, they narrowed the size distribution of oblate silver nanoparticles with a mean radius of 6 nm in ultrahigh vacuum using a tunable nanosecond laser. Laser irradiation leads to the evaporation of atoms preferentially at the edges of the oblate particles, transforming them into more spherical particles with an aspect ratio closer to 1. Successive tuning of the laser frequency can in this way be used to produce a homogeneous size distribution.

Not only has laser light been used to control the particle size and shape of nanoparticles prepared by various methods in solution, supported or embedded in a solid medium, but it has also been used to prepare metallic nanoparticles by laser irradiation of a metal target immersed in a liquid solution in the presence of stabilizing surfactants (134–139a,b). Mafune et al. (134a–e) combined the creation of gold nanoparticles by laser ablation in aqueous solution containing sodium dodecyl sulfate with subsequent fragmentation in order to produce size-selected gold nanoparticles. The ablation was carried out with 1064-nm laser light and the fragmentation was induced with 532 nm in resonance with the gold nanoparticle absorption. The size of the gold nanoparticles can be varied

Figure 5 (*a*) Transient absorption and ground state spectra of a 28-atom gold cluster recorded at different delay times after excitation with 400-nm femtosecond laser pulses. The inset shows the excited state dynamics observed at 600 nm. (*b*) Luminescence spectrum of the Au_{28} cluster after 532-nm excitation together with the ground state absorption spectrum.

between 1.7 and 5.5 nm and depends on the surfactant concentration and the laser fluence.

Using ultrashort femtosecond laser pulses has been found to have a great advantage over using longer nanosecond pulses. We found that the efficiency of the laser-induced melting is pulse-width dependent for gold nanorods irradiated at the absorption wavelength of the longitudinal surface plasmon band (133a,b). With nanosecond laser pulses the energy threshold for the complete melting of the gold nanorods is on the order of 100 times larger than when using femtosecond laser pulses. In addition, at higher pulse energies fragmentation of the nanorods is observed (see Figure 6*c*), whereas at lower pulse energies only an incomplete melting and a high abundance of odd-shaped particles are seen (133a,b). This leads to the conclusion that nanosecond pulses are less suitable for melting gold nanorods in colloidal solution compared to shorter laser pulses. A likely explanation for this observation is the fact that the cooling of the nanoparticles (on the order of hundreds of ps, see above) can compete with the heating of the particles when long pulses are used for excitation. In addition, the optical density of the sample may change during the pulse duration of several nanoseconds as the plasmon band shows strong bleaching initially after laser excitation.

We found (133a,b) that under controlled femtosecond pulse energies, colloidal gold nanorods are transformed into spherical particles (Figure 6*b*). Under these conditions, complete melting of the nanorods in solution into spheres of similar volume takes place without detectable fragmentation (as determined by TEM studies). We have found that the melting time for this process in solution is 30 ps (140). This time is slower than heating of the nanoparticle lattice by electron-phonon interactions ($\sim$1 ps) but faster than cooling of the lattice by heat transfer and conduction within the surrounding medium (100 ps).

The structural changes of the gold nanorods are accompanied by drastic changes in the optical absorption spectrum of these colloidal solutions (see Figures 6*f* and 6*g*). This in turn makes it easy to follow the structural changes once a correlation between the shape changes confirmed by TEM with the optical absorption spectrum is established. Energy thresholds for the onset of the melting can therefore be determined. In the specific case for gold nanorods, the longitudinal plasmon absorption disappears, whereas the intensity of the plasmon band at 520 nm (belonging to the transverse mode of rods as well as the surface plasmon absorption of spheres) increases because of the higher extinction coefficient of spherical particles. We were able to devise a spectroscopic method from which the amount of

Figure 6 Transmission electron microscopy (TEM) images of gold nanorods taken before (*a*) and after exposure to femtosecond (*b*) and nanosecond (*c*) laser pulses. (*d*) and (*e*) show the corresponding size distributions of the spherical nanoparticles obtained after laser excitation while (*f*) and (*g*) show the accompanying absorption spectra as a function of increasing laser pulses for femtosecond and nanosecond laser irradiation, respectively.

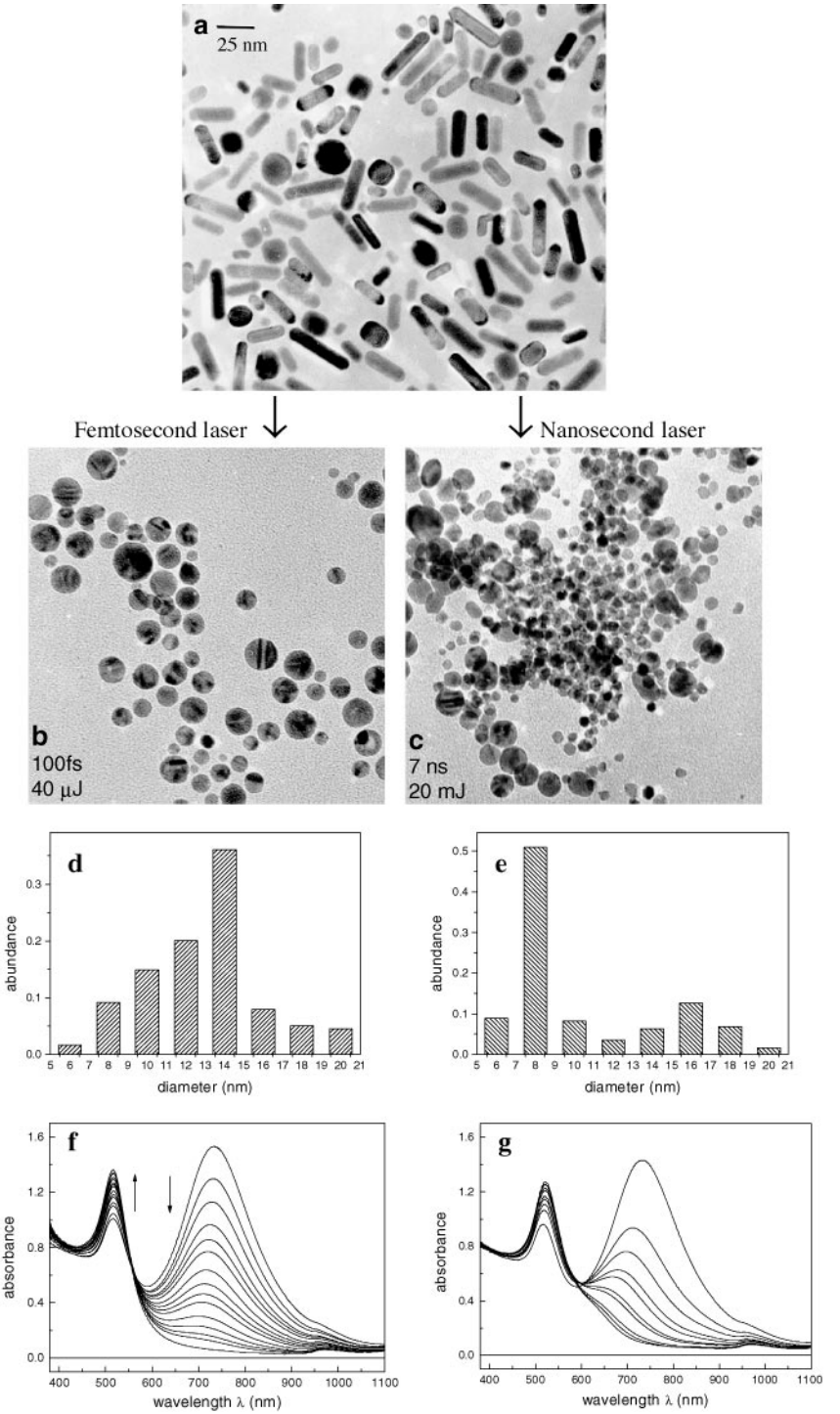

energy required to melt a nanorod is determined and found it to be in the tens of femtojoules (141).

We have investigated the mechanism of the femtosecond laser photothermal shape transformation from a nanorod single crystal to a nanodot with multitwin planes using high-resolution TEM (HRTEM) (142). Gold nanorods are defect free as prepared, and their surface contains the unstable {110} as well as the more stable {111} and {100} surfaces (143). We found that the first step in the shape transformation is the creation of defects in the interior of the nanorods resulting from partial melting. The point defects evolve into line defects and plane defects (twin planes). Simultaneously, the unstable {110} surface reconstructs into the more stable {111} and {100} surfaces. The spherical particles have only the {111} and {100} surfaces.

ASSEMBLY OF METAL NANOPARTICLES AND THEIR COLLECTIVE PROPERTIES

Whereas the properties of individual particles or a collection of well-separated particles in colloidal solution or for example in a sol-gel glass are of great interest to understand the fundamental properties of nanoparticles like their energy structure and relaxation mechanism, it has become more important in recent years to study the collective properties of assembled nanostructures (144–162a,b,c). In order to build practical devices with nanomaterials and to take advantage of the unique properties, the individual nanoparticles need to be linked together (assembled) in a desired fashion. Once it is possible to control the architecture of these artificial atoms composed of different materials, miniaturized electronic circuits consisting of metal-semiconductor or metal-insulator junctions could be built. Although it is possible today to synthesize nanoparticles of nearly any material and size, it remains a challenge to use these building blocks for manufacturing higher hierarchies. This can be considered as a bottoms-up approach in designing new functional materials. Much progress has been made in this field, and only a few examples of assembled nanoparticles and the change of their properties as a function of the particle size and shape and the interparticle distances can be given here. For more complete reviews the reader is referred to other references (5, 24, 28).

In order to introduce structure and a designed pattern to the assembly of nanoparticles already ordered, templates can be used to arrange the nanoparticles. One- and two-dimensional arrays of metallic nanorods have been fabricated by use of a porous aluminum oxide membrane as a template (53a–e). Gold or other metals are simply electrochemically deposited into the membranes, and the length of the rods is controlled by the deposition time. The separation between the nanoparticles is determined by the spacing of the pores in the template, which are formed by electrochemical etching. Hence the assembly of the nanostructures is determined by the template, and its synthesis with size control in the nanometer range becomes the crucial factor.

Nanolithography as developed by Van Duyne et al. (55) could also be regarded as a template method. Polystyrene nanoparticles are assembled to form a monolayer on a glass substrate (the material of the substrate can easily be varied). Gold or silver is then evaporated into the spaces between the polystyrene balls, which are subsequently removed. This gives rise to an ordered array of metallic nanoparticles. The size of the particles can be controlled by the size of the polystyrene spheres, and the shape can be controlled by the angle of incidence between the substrate and the material deposition beam (144). The dimensions of the two-dimensional order are determined by the assembly of the polystyrene nanoparticles and hence the template. It should be pointed out that these arrays consist of naked metallic clusters as no organic molecules are bound to them for interparticle separation. Schatz and coworkers (145) have accurately modeled the absorption spectra by the discrete dipole approximation and showed a strong dependence on the particle shape, substrate, and surrounding medium.

A very different template, which has been used for a three-dimensional assembly of mainly gold nanoparticles, is DNA (146a–c; 147). The DNA is modified with alkanethiol-capped oligonucleotides (single-stranded DNA), and the binding to complementary linker oligonucleotide (DNA) strands allows the formation of extended structures with control over particle chemical composition, periodicity, and aggregate thermal stability. Because of the recognition capability and therefore the high selectivity of DNA, this approach could also be categorized as a template approach. High control over the optical, mechanical, and electrical properties of these hybrid bioinorganic materials was demonstrated for gold nanoparticles with DNA independently by the groups of Mirkin (5; 146a–c) and Alivisatos (147) and was modeled again by Schatz (148) within the discrete dipole approximation.

Instead of using a template for the arrangement of nanoparticles, it has been shown by several authors (149–153) that nanoparticles with a very narrow size distribution form spontaneous self-assembly structures when deposited from a solution phase onto a solid substrate by carefully adjusting the rate of solvent evaporation. An electrophoretic deposition of colloidal gold (151) was also shown in one of the earlier works of a large-scale assembly of metallic nanoparticles. The success of this method depends mainly on the size distribution of the particles and how careful the solvent evaporation can be controlled by adjusting the temperature, vapor pressure, and particle concentration because this process is driven by thermodynamics. A kinetic product would correspond to the uncontrolled aggregation of the particles. The influence of the solvent evaporation process on the two- and three-dimensional assembly of silver nanoparticles from their solution phase has been studied in great detail by Pileni and coworkers (25; 152a,b).

This self-assembly method is not limited to spherical nanoparticles of gold, silver, and copper (150–153; 156–159a–c), but the assembly of nanorods has also been shown (153). Figure 7 shows the self-assembly of gold nanorods prepared by an electrochemical method. Nanoparticle concentration, solvent evaporation, narrow size distribution, ionic strength, and surfactant concentration were all found to be important parameters.

Although a narrow size distribution is thought to be required to form nanocrystal superlattices extending over large areas, it has been shown by Petroski et al. (154) that it is possible to form self-assembled monolayers of polydisperse platinum nanoparticles with different shapes (cubes, tetrahedrons, truncated octahedrons) by adding dodecanethiol as another capping material that replaces the acrylic acid with which the particles are capped during the synthesis (155). Figure 8 shows a TEM image of an assembled monolayer of platinum nanoparticles forming a hexagonally closed packed structure. Similarly, Kiely et al. (26, 156) have shown that it is possible to produce ordered arrays from a bimodal distribution of sizes of the same metal and also using different metals as they formed AB_2 and AB superlattice arrays consisting of gold and silver nanoparticles. In their case, the size distribution of each metal fraction (A or B) was very narrow.

Although the capping material or ligands are essential for the stability of the nanoparticles in solution, they also control the interparticle distances of self-assembled structures. In the examples about the platinum and mixed alloy structures given above, the particles were tethered together by strong binding ligands like alkanethiols that are commonly used because of their binding affinity to metals. It has been shown that the ligand molecules are interwoven by comparing the measured separation between two neighboring particles with twice the chain length of the ligand molecules (24, 25, 28, 149, 150). Therefore the nanoparticles cannot come too close to each other simply because of steric hindrance that can be controlled in a designed fashion by varying the chain length of the alkanethiols or alkanephosphines. In this manner, assembly of nanoparticles over a fairly large area (several microns) can be achieved. Even greater chemical control can be achieved by using bifunctional ligands (158), which are bound to the surface of the nanoparticles and can bind to a neighboring particle during the assembly process via the second functional group.

Although the proper choice of capping material turns out to be important in preparing nanostructure assemblies these organic molecules also determine the collective properties like the optical transmission as well as the electric conductance of the final material. This can be achieved either by the choice of the ligand material itself (a conducting polymer for example) or by control over the interparticle distances. Because the electronic wavefunction of the nanoparticles can extend beyond the physical boundaries of the particles, at a certain interparticle distance direct coupling between the particles takes place and the properties of the assembly will no longer be dominated by the properties of the isolated nanoparticles. This has been shown elegantly by Heath and coworkers (24; 159a–c), who prepared Langmuir monolayer films of organically functionalized 2–5-nm silver quantum dots where the interparticle distance can be controlled by the applied surface tension (pressure). They measured their collective behavior with a number of different techniques including linear reflectance and absorbance, second harmonic generation, and electronic transport measurement (DC resistivity, STM tunneling). They found the collective properties are strongly dependent on the distance between neighboring particles as well as the particle diameter. When the particle separation

becomes less than 0.5 nm an insulator-to-metal transition is observed for 4-nm particles by a sharp discontinuity in the second harmonic response and a reflectance resembling bulk silver as well as a metallic-like Ohmic resistance behavior.

The wet chemical approach of spontaneous and directed assembly for two-dimensional structures can easily be extended to form three-dimensional multilayer superlattices by repeating the process for the self-assembly or by starting with a higher particle concentration. In a slightly different approach, a linker molecule is first assembled on a substrate (preferably dithiol molecules are assembled on a gold substrate for example). A monolayer of nanoparticles is then assembled and covered with another layer of dithiols upon which another layer of nanoparticles can be prepared. In this method, alternating layers of nanoparticles of different size as well as different composition can be used, as shown by Rao and coworkers (160) as well as by Natan and coworkers (161). Studies were performed regarding the collective optical and conductive properties as a function of the number of deposited layers as well as the nature of the crosslinker. Feldstein et al. (99) measured the femtosecond electron dynamics (as described in detail above) for such a film and found that the electron-phonon relaxation time increases with increasing film thickness.

A slightly different approach for the synthesis of three-dimenisonal structures by layer-by-layer fabrication has been undertaken by Mulvaney and coworkers (27; 162a–c), who coated spherical gold nanoparticles with a shell of SiO_2. Films were then manufactured on a glass substrate by repeated dipping of the substrate into a solution containing the particles. Each cycle produced approximately one monolayer as verified by AFM. The optical absorption spectra depend on the filling factor (percentage of the gold to total material, which in turn is determined by the SiO_2 shell thickness) and can be modeled accurately with Maxwell-Garnett theory. In the limit of a very thin shell, the films display bulk metallic optical properties, whereas for a large shell thickness the individual plasmon absorption is preserved allowing for an overall continuous tunability of the optical properties of the composite films.

APPLICATIONS OF METAL NANOPARTICLES AS SENSORS

The sensitivity of the plasmon resonance on the local environment through surface-adsorbed molecules or induced by decreased interparticle separations and particle-particle coupling has led to an increased effort in building sensor devices based on metallic nanoparticles. Both the optical properties as well as the conductivity of nanocomposites as illustrated above can be used as a sensitive monitoring property. The following discussion gives a few examples of how noble metal nanoparticles have been used as chemical specific sensors.

Because of its biocompatibility, gold nanoparticles have been used in a variety of biological sensing applications. Mirkin and coworkers (146a–c) designed a highly

selective polynucleotide detection method based on mercaptoalkyloligonucleotide-modified gold nanoparticles. Hybridization of covalently attached probe segments with the target oligonucleotide leads to aggregation, which results in a sensitive color change from red to purple indicating interparticle coupling. The aggregation and dissociation is reversible, and the observed temperature range for "melting" is unusually narrow. This approach allows the detection of 10 femtomoles of an oligonucleotide. A modification of this technique exploiting the sequence-selective binding of DNA to oligonucleotide-modified gold nanoparticles as probes has been reported by the same group (163). Instead of monitoring an optical color change, however, the binding events localize the gold nanoparticles in an electrode gap, which allows the measurement of the conductivity changes. Because the electrode gaps were manufactured by photolithography on a Si wafer this sensing allows massive multiplexing with a detection limit for target DNA as low as 500 femtomole with a point mutation selectivity factor of about 100,000:1.

In a similar approach, which is less related to sensors but shows the capability of DNA-nanoparticle structures, a remote electronic control of DNA hybridization has been demonstrated recently by Hamad-Schifferli et al. (164). Inductive coupling of a radio-frequency magnetic field to a metal nanoparticle, which is covalently linked to DNA, increases the local temperature of the bound DNA, thereby inducing denaturation while leaving the surrounding molecules relatively unaffected. They showed high spatial localization of the denaturation, which might allow, in the future, controlling portions of proteins or nucleic acids while the rest of the molecule and neighboring species would remain relatively unaffected.

Protein structural characterization can be carried out by Raman spectroscopy and especially SERS. Keating et al. (84a,b) have designed a system that shows high sensitivity by sandwiching the protein molecule between a metal nanoparticle and a metal surface or an aggregated sol commonly used as a substrate for SERS. They demonstrated for cytochrome c, which is covalently attached to gold nanoparticles, that the protein orientation with respect to the SERS substrate could be controlled, although the protein retains its native conformation. The orientation of the heme is more stable in this metal-protein-metal configuration compared to the adsorption of the protein to the SERS substrate alone, and this allows one to probe otherwise buried chromophores.

A chemical vapor-sensing device was designed by Vossmeyer et al. (165a,b). A thin film resistor was fabricated from gold nanoparticles linked to different types of organic dendrimers by layer-by-layer self-assembly. The presence of the nanoparticles provides the film with electric conductivity, whereas the dendrimers serve as cross linkers and provide sites for selective binding of analyte vapor molecules. After exposure of the film to toluene, 1-propanol, and water vapors, the conductivity of the film is significantly decreased, with the chemical selectivity determined by the solubility properties of the dendrimers.

A colometric approach similar to the one already described above for DNA was recently used to probe for heavy metal ions, including toxic metals such as lead,

cadmium, and mercury (166). The method is based on 11-mercaptoundecanoic acid functionalized gold particles, which are aggregated in solution in the presence of divalent ions by an ion-templated chelation process. Aggregation causes the known change in the absorption spectrum (broadening and redshift) as well as an enhanced hyper-Rayleigh scattering response, which is more sensitive than optical absorption measurements. The sensitivity of this colometric method is not only based on the pronounced color change from red to blue for aggregated gold nanoparticles but also takes advantage of the large extinction coefficient of metallic nanoparticles compared to commonly used fluorescence labels.

ACKNOWLEDGMENTS

The authors wish to acknowledge the financial support of the Division of Materials Research of the National Science Foundation (grant # 0138391).

The *Annual Review of Physical Chemistry* is online at http://physchem.annualreviews.org

LITERATURE CITED

1. Henglein A. 1993. *J. Phys. Chem.* 97: 8457
2. Brus LE. 1991. *Appl. Phys. A* 53:465
3a. Alivisatos AP. 1996. *Science* 271:933
3b. Alivisatos AP. 1996. *J. Phys. Chem.* 100:13226
4. Mulvaney P. 1996. *Langmuir* 12:788
5. Storhoff JJ, Mirkin CA. 1999. *Chem. Rev.* 99:1849
6. Schmid G, Chi LF. 1998. *Adv. Mater.* 10:515
7. Alivisatos AP, Barbara PF, Castleman AW, Chang J, Dixon DA, et al. 1998. *Adv. Mater.* 10:1297
8. Heath JR, Shiang JJ. 1998. *Chem. Soc. Rev.* 27:65
9a. Link S, El-Sayed MA. 1999. *J. Phys. Chem. B* 103:8410
9b. Link S, El-Sayed MA. 2000. *Int. Rev. Phys. Chem.* 19:409
9c. El-Sayed MA. 2001. *Acc. Chem. Res.* 34:257 and references therein
10. Schmid G. 1994. *Clusters and Colloids: From Theory to Application*. Weinheim: VCH
11. Kamat PV, Meisel D. 1997. *Studies in Surface Science and Catalysis*, Vol. 103. *Semiconductor Nanoclusters—Physical, Chemical, and Catalytic Aspects*. Amsterdam: Elsevier
12. Edelstein AS, Cammarata RC. 1996. *Nanoparticles: Synthesis, Properties and Applications*. Bristol: Inst. Phys.
13. Hagfeldt A, Graetzel M. 2000. *Acc. Chem. Res.* 33:269
14. Aiken JD III, Finke RG. 1999. *J. Mol. Catal. A* 145:1 and references therein
15. Reetz MT, Quaiser SA, Breinbauer R, Teshe B. 1995. *Angew. Chem. Int. Ed. Engl.* 34:2728
16. Boennemann H, Braun G, Brijoux W, Brinkmann R, Schulze Tilling A, et al. 1996. *J. Organomet. Chem.* 520:143
17. Kreibig U, Vollmer M. 1995. *Optical Properties of Metal Clusters*. Berlin: Springer
18. Kerker M. 1969. *The Scattering of Light and Other Electromagnetic Radiation*. New York: Academic
19. Bohren CF, Huffman DR. 1983. *Absorption and Scattering of Light by Small Particles*. New York: Wiley

20. Papavassiliou GC. 1979. *Prog. Solid State Chem.* 12:185
21. Kerker M. 1985. *J. Colloid Interface Sci.* 105:297
22. Faraday M. 1857. *Philos. Trans.* 147: 145
23. Mie G. 1908. *Ann. Phys.* 25:329
24. Collier CP, Vossmeyer T, Heath JR. 1998. *Annu. Rev. Phys. Chem.* 49:371
25. Pileni M. 2001. *J. Phys. Chem. B* 105:3358
26. Brust M, Kiely CJ. 2002. *Colloids Surf. A* 202:175
27. Mulvaney P. 2001. *MRS Bull.* 1009
28. Wang ZL. 1998. *Adv. Mater.* 10:13
29. Creighton JA, Eadon DG. 1991. *J. Chem. Soc. Faraday Trans.* 87:3881
30. Ashcroft NW, Mermin ND. 1976. *Solid State Physics.* Philadelphia: Saunders College
31a. Alvarez MM, Khoury JT, Schaaff TG, Shafigullin MN, Vezmer I, Whetten RL. 1997. *J. Phys. Chem. B* 101:3706
31b. Schaaff TG, Shafigullin MN, Khoury JT, Vezmer I, Whetten RL, et al. 1997. *J. Phys. Chem. B* 101:7885
32. Hostetler MJ, Wingate JE, Zhong CJ, Harris JE, Vachet RW, et al. 1998. *Langmuir* 14:17
33. Deleted in proof
33a. Kreibig U, Genzel U. 1985. *Surf. Sci.* 156:678
33b. Kreibig U, von Fragstein C. 1969. *Z. Phys.* 224:307
33c. Kreibig U. 1970. *Z. Phys.* 234:307
34. Ruppin R, Yatom H. 1976. *Phys. Status Solidi B* 74:647
35. Kawabata A, Kubo R. 1966. *J. Phys. Soc. Jpn.* 21:1765
36. Hache F, Ricard D, Flytzanis C. 1986. *J. Opt. Am. Soc. B* 3:1647
37. Cini M. 1981. *J. Opt. Soc. Am.* 71:386
38. Genzel L, Martin TP, Kreibig U. 1975. *Z. Phys. B* 21:339
39. Wood DM, Ashcroft NW. 1982. *Phys. Rev. B* 25:6255
40. Kraus WA, Schatz GC. 1983. *J. Chem. Phys.* 79:6130
41. Yannouleas C, Broglia RA. 1992. *Ann. Phys.* 217:105
42. Brack M. 1993. *Rev. Mod. Phys.* 65:677
43. Bonacic-Koutecky V, Fantucci P, Koutecky J. 1991. *Chem. Rev.* 91:1035
44. Persson NJ. 1993. *Surf. Sci.* 281:153
45a. Palpant B, Prevel B, Lerme J, Cottancin E, Pellarin M, et al. 1998. *Phys. Rev. B* 57:1963
45b. Lerme J, Palpant B, Prevel B, Cottancin E, Pellarin M, et al. 1998. *Eur. Phys. J. D* 4:95
46. Gans R. 1915. *Ann. Phys.* 47:270
47. van der Zande BMI, Bohmer MR, Fokkink LGJ, Schonenberger C. 1997. *J. Phys. Chem. B* 101:852
48. Yu YY, Chang SS, Lee CL, Wang CRC. 1997. *J. Phys. Chem. B* 101:6661
49. Mohamed MB, Ismael KZ, Link S, El-Sayed MA. 1998. *J. Phys. Chem. B* 102:9370
50. Link S, Wang ZL, El-Sayed MA. 1999. *J. Phys. Chem. B* 103:3529
51. Deleted in proof
51a. Kreibig U, Althoff A, Pressmann H. 1981. *Surf. Sci.* 106:308
51b. Quinten M, Kreibig U. 1986. *Surf. Sci.* 172:557
51c. Quinten M, Schoenauer D, Kreibig U. 1989. *Z. Phys. D* 26:239
52. Maxwell-Garnett JC. 1904. *Philos. Trans. R. Soc. London* 203:385
53a. Foss CA, Hornyak GL, Tierney MJ, Martin CR. 1992. *J. Phys. Chem.* 96:9001
53b. Hornyak GL, Patrissi CJ, Martin CR. 1997. *J. Phys. Chem. B* 101:1548
53c. Foss CA, Hornyak GL, Stockert JA, Martin CR. 1992. *J. Phys. Chem.* 96: 7497
53d. Foss CA, Hornyak GL, Stockert JA, Martin CR. 1994. *J. Phys. Chem.* 98:2963
53e. Hornyak GL, Martin CR. 1997. *Thin Solid Films* 303:84
54. Schatz GC. 2001. *J. Mol. Struct. THEOCHEM* 573:73 and references therein
55. Haynes CL, Van Duyne RP. 2001. *J. Phys. Chem. B* 105:5599

56. Jin R, Cao YW, Mirkin CA, Kelly KL, Schatz GC, Zheng JG. 2001. *Science* 294:1901
57. Heilweil EJ, Hochstrasser RM. 1985. *J. Chem. Phys.* 82:4762
58. Soennichsen C, Franzl T, Wilk G, von Plessen G, Feldmann J, et al. 2002. *Phys. Rev. Lett.* 88:77402
59a. Lehmann J, Nerschdorf M, Pfeiffer W, Thon A, Voll S, Gerber G. 2000. *Phys. Rev. Lett.* 85:2921
59b. Lehmann J, Nerschdorf M, Pfeiffer W, Thon A, Voll S, Gerber G. 2000. *J. Chem. Phys.* 112:5428
60. Link S, El-Sayed MA. 1999. *J. Phys. Chem. B* 103:4212
61a. Lamprecht B, Leitner A, Aussenegg FR. 1997. *Appl. Phys. B* 64:269
61b. Lamprecht B, Leitner A, Aussenegg FR. 1999. *Appl. Phys. B* 68:419
62. Liau YH, Unterreiner AN, Chang Q, Scherer NF. 2001. *J. Phys. Chem. B* 105:2135
63. Klar T, Perner M, Grosse S, von Plessen G, Spirkl W, Feldmann J. 1998. *Phys. Rev. Lett.* 80:4249
64. Itoh T, Asahi T, Masuhara H. 2002. *Jpn. J. Appl. Phys.* 41:L76
65. Soennichsen C, Geier S, Hecker NE, von Plessen G, Feldmann J, et al. 2000. *Appl. Phys. Lett.* 77:2949
66. Deleted in proof
66a. Hoevel H, Fritz S, Hilger A, Kreibig U, Vollmer M. 1993. *Phys. Rev. B* 48: 18178
66b. Kreibig U, Gartz M, Hilger A. 1997. *Ber. Bunsenges. Phys. Chem.* 101:1593
67a. Stietz F, Bosbach J, Wenzel T, Varanyan T, Goldman A, Traeger F. 2000. *Phys. Rev. Lett* 84:5644
67b. Varanyan T, Simon M, Traeger T. 1999. *Appl. Phys. B* 68:425
67c. Varanyan T, Bosbach J, Stietz F, Traeger T. 2000. *Appl. Phys. B* 73:391
68. Mooradian A. 1969. *Phys. Rev. Lett.* 22:185
69. Whittle DG, Burstein E. 1981. *Bull. Am. Phys. Soc.* 26:777
70. Boyd GT, Yu ZH, Shen YR. 1986. *Phys. Rev. B* 33:7923
71. Moshovists M. 1985. *Rev. Mod. Phys.* 57:783
72. Heritage JP, Bergman JG, Pinczuk A, Worlock JM. 1979. *Chem. Phys. Lett.* 67:229
73. Apell P, Monreal R. 1988. *Phys. Scr.* 38:174
74. Plekhanov VG, Siliukova TV. 1990. *Sov. Phys. Solid State* 32:1268
75a. Chen CK, Heinz TF, Ricard D, Shen YR. 1983. *Phys. Rev. B* 27:1965
75b. Boyd GT, Rasing T, Leite JRR, Shen YR. 1984. *Phys. Rev. B* 30:519
76. Mohamed MB, Volkov VV, Link S, El-Sayed MA. 2000. *Chem. Phys. Lett.* 317:517
77. Wilcoxon JP, Martin JE, Parsapour F, Wiedenman B, Kelley DF. 1998. *J. Chem. Phys.* 108:9137
78. Varnavski O, Ispasoiu RG, Balogh L, Tomalia D, Goodson T III. 2001. *J. Chem. Phys.* 114:1962
79a. Otto A. 1991. *J. Raman Spectr.* 22:743
79b. Otto A, Mrozek I, Grabhorn H, Akeman W. 1992. *J. Phys. Condens. Matter* 4:1143
80a. Zeman EJ, Schatz GC. 1987. *J. Phys. Chem.* 91:634
80b. Schatz GC. 1984. *Acc. Chem. Res.* 17:370
81. Campion A. 1998. *Chem. Soc. Rev.* 4: 241
82. Creighton JA, Blatchford CG, Albrecht MG. 1979. *J. Chem. Soc. Faraday II* 75:790
83. Hildebrandt P, Stockburger M. 1984. *J. Phys. Chem.* 88:5935
84a. Keating CD, Kovaleski KM, Natan MJ. 1998. *J. Phys. Chem. B* 102:9404
84b. Keating CD, Kovaleski KM, Natan MJ. 1998. *J. Phys. Chem. B* 102:9414
85. Deleted in proof
85a. Nie S, Emory SR. 1997. *Science* 275: 1102
85b. Emory SR, Haskins WE, Nie S. 1998. *J. Am. Chem. Soc.* 120:8009

85c. Krug JT, Wang GD, Emory SR, Nie S. 1999. *J. Am. Chem. Soc.* 121:9208
85d. Doering WE, Nie S. 2002. *J. Phys. Chem. B* 106:311
86. Deleted in proof
86a. Kneipp K, Wang Y, Kneipp H, Perelman LV, Itzkan I, et al. 1997. *Phys. Rev. Lett.* 78:1667
86b. Kneipp K, Kneipp H, Itzkan I, Dasari RR, Feld MS. 1999. *Chem. Phys.* 247:155
86c. Kneipp K, Kneipp H, Itzkan I, Dasari RR, Feld MS. 2002. *J. Phys. Condens. Matter* 14:R597
87a. Michaels AM, Nirmal M, Brus LE. 1999. *J. Am. Chem. Soc.* 121:9932
87b. Michaels AM, Jiang J, Brus LE. 2000. *J. Phys. Chem. B* 104:11965
88. Xu H, Bjerneld EJ, Kall M, Borjesson L. 1999. *Phys. Rev. Lett.* 83:4357
89a. Nikoobakht B, El-Sayed MA. 2002. *Chem. Phys. Lett.* 366:17
89b. Deleted in proof
90. Oldenburg SJ, Westcott SL, Averitt RD, Halas NJ. 1999. *J. Chem. Phys.* 111:4729
91. Voisin C, Del Fatti N, Christofilos D, Vallee F. 2001. *J. Phys. Chem. B* 105: 2264 and references therein
92. Bigot JY, Halte V, Merle JC, Daunois A. 2000. *Chem. Phys.* 251:181
93. Stagira S, Nisoli M, De Silvestri S, Stella A, Tognini P, et al. 2000. *Chem. Phys.* 251:259
94. Perner M, Bost P, von Plessen G, Feldmann J, Becker U, et al. 1997. *Phys. Rev. Lett.* 78:2192
95. Hodak JH, Henglein A, Hartland GV. 2000. *J. Phys. Chem. B* 104:9954 and references therein
96a. Link S, Burda C, Wang ZL, El-Sayed MA. 1999. *J. Chem. Phys.* 111:1255
96b. Link S, Burda C, Mohamed MB, Nikoobakht B, El-Sayed MA. 2000. *Phys. Rev. B* 61:6086
97. Roberti TW, Smith BA, Zhang JZ. 1995. *J. Chem. Phys.* 102:3860
98. Hamanaka Y, Hayashi N, Nakamura A, Omi S. 1998. *J. Lumin.* 76/77:221
99. Feldstein MJ, Keating CD, Liau YH, Natan MJ, Scherer NF. 1997. *J. Am. Chem. Soc.* 119:6638
100. Inouye H, Tanaka K, Tanahashi I, Hirao K. 1998. *Phys. Rev. B* 57:11334
101. Tokizaki T, Nakamura A, Kaneko S, Uchida K, Omi S, et al. 1994. *Appl. Phys. Lett.* 65:941
102. Averitt RD, Westcott SL, Halas NJ. 1998. *Phys. Rev. B* 58:10203
103. Sasai J, Kazuyuki H. 2001. *J. Appl. Phys.* 89:4548
104. Sun CK, Vallee F, Acioli LH, Ippen EP, Fujimoto JG. 1994. *Phys. Rev. B* 50:15337
105. Del Fatti N, Voisin C, Achermann M, Tzortzakis S, Christofilos D, Vallee F. 2000. *Phys. Rev. B* 61:16956
106. Voisin C, Christofilos D, Del Fatti N, Vallee F, Prevel B, et al. 2000. *Phys. Rev. Lett.* 85:2200
107. Belotskii ED, Tomchuk PM. 1992. *Int. J. Electron* 73:915
108. Hodak JH, Henglein A, Hartland GV. 2000. *J. Chem. Phys.* 112:5942
109. Stella A, Nisoli M, De Silvestri S, Svelto O, Lanzani G, et al. 1996. *Phys. Rev. B* 53:15497
110. Del Fatti N, Flytzanis C, Vallee F. 1999. *Appl. Phys. B* 68:433
111. Hu M, Hartland GV. 2002. *J. Phys. Chem. B* 106:7029
112a. Link S, Furube A, Mohamed MB, Asahi T, Masuhara H, El-Sayed MA. 2002. *J. Phys. Chem. B* 106:945
112b. Mohamed MB, Ahmadi TS, Link S, Braun M, El-Sayed MA. 2001. *Chem. Phys. Lett.* 343:55
113. Halte V, Bigot JY, Palpant B, Broyer M, Prevel B, Perez A. 1999. *Appl. Phys. Lett.* 75:3799
114. Westcott SL, Averitt RD, Wolfgang JA, Nordlander P, Halas NJ. 2001. *J. Phys. Chem. B* 105:9913
115a. Hodak JH, Martini I, Hartland GV. 1998. *J. Chem. Phys.* 108:9210
115b. Hodak JH, Henglein A, Hartland GV. 1999. *J. Chem. Phys.* 111:8613

115c. Hartland GV. 2002. *J. Chem. Phys.* 116:8048
115d. Hartland GV, Hu M, Wilson O, Mulvaney P, Sader JE. 2002. *J. Phys. Chem. B* 106:743
116. Del Fatti N, Voisin C, Chevy F, Vallee F, Flytzanis C. 1999. *J. Chem. Phys.* 110:11484
117. Perner M, Gresillon S, Marz J, von Plessen G, Feldmann J, et al. 2000. *Phys. Rev. Lett.* 85:792
118a. Qian W, Lin L, Deng YJ, Xia ZJ, Zou YH, Wong GKL. 2000. *J. Appl. Phys.* 87:612
118b. Qian W, Yan H, Wang JJ, Zou YH, Lin L, Wu JL. 1999. *Appl. Phys. Lett.* 74:1806
119. Brust M, Fink J, Bethell D, Schiffrin DJ, Kiely C. 1995. *J. Chem. Soc. Chem. Commun.*, p. 1655
120. Chen SW, Ingram RS, Hostetler MJ, Pietron JJ, Murray RW, et al. 1998. *Science* 280:2098
121. Schaaff TG, Knight G, Shafigullin M, Borkman RF, Whetten RL. 1998. *J. Phys. Chem. B* 102:10643
122. Link S, Beeby A, FitzGerald S, El-Sayed MA, Schaaff TG, Whetten RL. 2002. *J. Phys. Chem. B* 106:3410
123. Link S, El-Sayed MA, Schaaff TG, Whetten RL. 2002. *Chem. Phys. Lett.* 356:240
124. Schmid G. 1992. *Chem. Rev.* 92:1709
125. Smith BA, Zhang JZ, Giebel U, Schmid G. 1997. *Chem. Phys. Lett.* 270:139
126. Valden M, Lai X, Goodman DW. 1998. *Science* 281:1647
127a. Kurita H, Takami A, Koda S. 1998. *Appl. Phys. Lett.* 72:789
127b. Takami A, Kurita H, Koda S. 1999. *J. Phys. Chem. B* 103:1226
128. Stepanov AL, Hole DE, Bukharaev AA, Townsend PD, Nurgazizov NI. 1998. *Appl. Surf. Sci.* 136:298
129. Kamat PV, Flumiani M, Hartland GV. 1998. *J. Phys. Chem. B* 102:3123
130. Chang SS, Shih CW, Chen CD, Lai WC, Wang CRC. 1999. *Langmuir* 15:701
131. Kaempfe M, Rainer T, Berg KJ, Seifert G, Graener H. 1999. *Appl. Phys. Lett.* 74:1200
132a. Bosbach J, Martin D, Stietz F, Wenzel T, Traeger F. 1999. *Appl. Phys. Lett.* 74:2605
132b. Wenzel T, Bosbach J, Goldmann A, Stietz F, Traeger F. 1999. *Appl. Phys. B* 69:513
133a. Link S, Burda C, Mohamed MB, Nikoobakht B, El-Sayed MA. 1999. *J. Phys. Chem. A* 103:1165
133b. Link S, Burda C, Nikoobakht B, El-Sayed MA. 2000. *J. Phys. Chem. B* 104:6152
134a. Mafune F, Kohno JY, Takeda Y, Kondow T. 2002. *J. Phys. Chem. B* 106:7575
134b. Mafune F, Kohno JY, Takeda Y, Kondow T. 2001. *J. Phys. Chem. B* 105:9050
134c. Mafune F, Kohno JY, Takeda Y, Kondow T, Schwabe H. 2001. *J. Phys. Chem. B* 105:5114
134d. Mafune F, Kohno JY, Takeda Y, Kondow T, Schwabe H. 2000. *J. Phys. Chem. B* 104:9111
134e. Mafune F, Kohno JY, Takeda Y, Kondow T, Schwabe H. 2000. *J. Phys. Chem. B* 104:8333
135. Geohegan DB, Puretzky AA, Duscher G, Pennycook SJ. 1998. *Appl. Phys. Lett.* 72:2987
136. Lowndes DH, Rouleau CM, Thundat T, Duscher G, Kenik EA, Pennycook SJ. 1998. *Appl. Surf. Sci.* 129:355
137. Sasaki T, Terauchi S, Koshizaki N, Umehara H. 1998. *Appl. Surf. Sci.* 129:398
138. Paszti Z, Horvath ZE, Peto G, Karacs A, Guczi L. 1997. *Appl. Surf. Sci.* 110: 67
139a. Simakin AV, Voronov VV, Shafeev GA, Brayner R, Bozon-Verduraz F. 2001. *Chem. Phys. Lett.* 348:182
139b. Dolgaev SI, Simakin AV, Voronov VV, Shafeev GA, Brayner R, Bozon-Verduraz F. 2000. *Appl. Surf. Sci.* 186: 546
140. Link S, Burda C, Nikoobakht B, El-Sayed MA. 1999. *Chem. Phys. Lett.* 315:12

141. Link S, El-Sayed MA. 2001. *J. Chem. Phys.* 114:2362
142. Link S, Wang ZL, El-Sayed MA. 2000. *J. Phys. Chem. B* 104:7867
143. Wang ZL, Mohamed MB, Link S, El-Sayed MA. 1999. *Surf. Sci.* 440:L809
144. Deleted in proof
144a. Hulteen JC, Treichel DA, Van Duyne RP. 1995. *J. Vac. Sci. Technol. A* 13:1553
144b. Haynes CL, McFarland AD, Smith MT, Hulteen JC, Van Duyne RP. 2002. *J. Phys. Chem. B* 106:1898
145. Jensen TR, Schatz GC, Van Duyne RP. 1999. *J. Phys. Chem. B* 103:2394
146a. Elghanian R, Storhoff JJ, Mucic RC, Letsinger RL, Mirkin CA. 1997. *Science* 277:1078
146b. Mitchell GP, Mirkin CA, Letsinger RL. 1999. *J. Am. Chem. Soc.* 121:8122
146c. Taton TA, Mirkin CA, Letsinger RL. 2000. *Science* 289:1757
147. Alivisatos AP, Johnsson KP, Peng X, Wilson TE, Loweth CJ, et al. 1996. *Nature* 382:609
148. Storhoff JJ, Lazarides AA, Mucic RC, Mirkin CA, Letsinger RL, Schatz GC. 1999. *J. Am. Chem. Soc.* 122:4640
149. Korgel BA, Fullam S, Connolly S, Fitzmaurice D. 1998. *J. Phys. Chem. B* 102:8379
150. Deleted in proof
150a. Harfenist SA, Wang ZL, Alvarez MM, Vezmar I, Whetten RL. 1996. *J. Phys. Chem.* 100:13904
150b. Whetten RL, Khoury JT, Alvarez MM, Murthy S, Vezmar I, et al. 1996. *Adv. Mater.* 8:428
151. Giersig M, Mulvaney P. 1993. *J. Phys. Chem.* 97:6334
152a. Pileni MP. 1997. *Langmuir* 13:3266
152b. Pileni MP. 1998. *New J. Chem.* 22:693
153. Nikoobakht B, Wang ZL, El-Sayed MA. 2000. *J. Phys. Chem. B* 104:8635
154. Petroski JM, Green TC, El-Sayed MA. 2001. *J. Phys. Chem. A* 105:5542
155. Ahmadi TS, Wang ZL, Green TC, El-Sayed MA. 1996. *Science* 272: 1924
156. Kiely CJ, Fink J, Zheng JG, Brust M, Bethell D, Schiffrin DJ. 2000. *Adv. Mater.* 12:640
157. Fendler JH. 1996. *Chem. Mater.* 8:1616
158. Andres RP, Bielefeld JD, Henderson JI, Janes DB, Kolagunta VR, et al. 1996. *Science* 273:1690
159a. Collier CP, Saykally RJ, Shiang JJ, Henrichs SE, Heath JR. 1997. *Science* 277:1978
159b. Kim SH, Medeiros-Ribeiro G, Ohlberg DAA, Williams RS, Heath JR. 1999. *J. Phys. Chem. B* 103:10341
159c. Sampaio JF, Beverly KC, Heath JR. 2001. *J. Phys. Chem. B* 105:8797
160. Rao CNR, Kulkarni GU, Thomas PJ, Edwards PP. 2000. *Chem. Soc. Rev.* 29: 27
161. Musick MD, Keating CD, Lyon LA, Botsko SL, Pena DJ, et al. 2000. *Chem. Mater.* 12:2869
162. Oldfield G, Ung T, Mulvaney P. 2000. *Adv. Mater.* 12:1519
163. Park SJ, Taton TA, Mirkin CA. 2002. *Science* 295:1503
163c. Ung T, Liz-Marzan LM, Mulvaney P. 2001. *J. Phys. Chem. B* 105:3441
164. Hamad-Schifferli K, Schwartz JJ, Santos AT, Zhang S, Jacobson JM. 2002. *Nature* 415:152
165a. Vossmeyer T, Guse B, Besnard I, Bauer RE, Mullen K, Yasuda A. 2002. *Adv. Mater.* 14:238
165b. Krasteva N, Besnard I, Guse B, Bauer RE, Mullen K, et al. 2002. *Nano Lett.* 2:551
166. Kim YJ, Johnson RC, Hupp JT. 2001. *Nano Lett.* 1:165

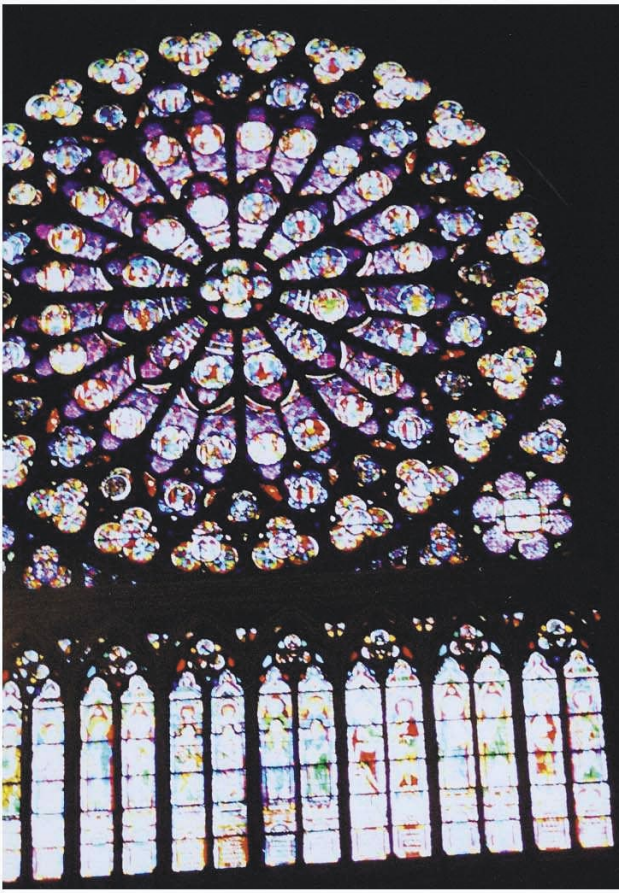

Figure 1 Rose window of the Cathedral of Notre Dame, Paris 2002.

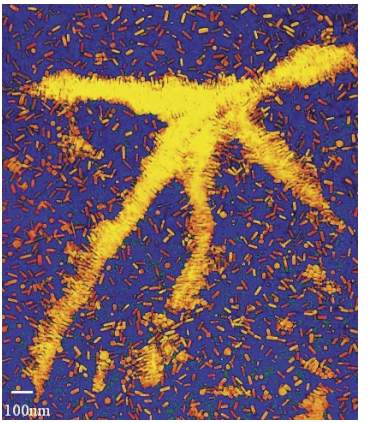

Figure 7 TEM image of a self-assembly formed from colloidal gold nanorods on a carbon covered copper grid.

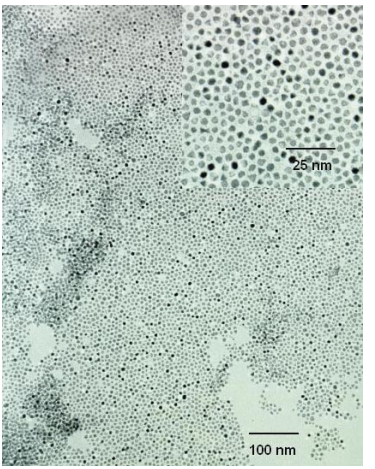

Figure 8 TEM image of a self-assembled monolayer of platinum nanoparticles having different shapes. The inset is an enlarged region showing the short range order of the nanoparticles.

Annual Review of Physical Chemistry
Volume 54, 2003

CONTENTS

Frontispiece—*Richard Bersohn* xiv

SOME PLEASURES IN CHEMICAL PHYSICS, *Richard Bersohn* 1

IN SEARCH OF PERFECTION: UNDERSTANDING THE HIGHLY DEFECT-SELECTIVE CHEMISTRY OF ANISOTROPIC ETCHING, *Melissa A. Hines* 29

LONG-RANGE RESONANCE ENERGY TRANSFER IN MOLECULAR SYSTEMS, *Gregory D. Scholes* 57

FEMTOSECOND TIME-RESOLVED PHOTOELECTRON SPECTROSCOPY OF POLYATOMIC MOLECULES, *Albert Stolow* 89

ORGANIC ATMOSPHERIC PARTICULATE MATERIAL, *John H. Seinfeld and James F. Pankow* 121

CONJUGATED POLYMERS AS MOLECULAR MATERIALS: HOW CHAIN CONFORMATION AND FILM MORPHOLOGY INFLUENCE ENERGY TRANSFER AND INTERCHAIN INTERACTIONS, *Benjamin J. Schwartz* 141

MOLECULAR ASPECTS OF HALIDE ION HYDRATION: THE CLUSTER APPROACH, *William H. Robertson and Mark A. Johnson* 173

STATE-RESOLVED DYNAMICS OF PHOTOFRAGMENTATION, *Yuan-Pern Lee* 215

MASTER EQUATION MODELS FOR CHEMICAL REACTIONS OF IMPORTANCE IN COMBUSTION, *Michael J. Pilling and Struan H. Robertson* 245

OPTICAL DIAGNOSTICS FOR THIN FILM PROCESSING, *Irving P. Herman* 277

STM CONTROL OF CHEMICAL REACTIONS: SINGLE-MOLECULE SYNTHESIS, *Saw-Wai Hla and Karl-Heinz Rieder* 307

OPTICAL PROPERTIES AND ULTRAFAST DYNAMICS OF METALLIC NANOCRYSTALS, *Stephan Link and Mostafa A. El-Sayed* 331

THEORY OF DIPOLE-BOUND ANIONS, *Kenneth D. Jordan and Feng Wang* 367

PHOTOELECTRON ANGULAR DISTRIBUTIONS, *Katharine L. Reid* 397

TWO-DIMENSIONAL FEMTOSECOND SPECTROSCOPY, *David M. Jonas* 425

TUNNELING AND OPTICAL SPECTROSCOPY OF SEMICONDUCTOR NANOCRYSTALS, *Uri Banin and Oded Millo* 465

QUANTUM SCATTERING CALCULATIONS ON CHEMICAL REACTIONS, *Stuart C. Althorpe and David C. Clary* 493

STRUCTURAL STUDIES OF BIOMATERIALS USING DOUBLE-QUANTUM SOLID-STATE NMR SPECTROSCOPY, *G.P. Drobny, J.R. Long, T. Karlsson, W. Shaw, J. Popham, N. Oyler, P. Bower, J. Stringer, D. Gregory, M. Mehta, and P.S. Stayton* 531

INDEXES

Subject Index 573

Cumulative Index of Contributing Authors, Volumes 50–54 597

Cumulative Index of Chapter Titles, Volumes 50–54 600

ERRATA

An online log of corrections to *Annual Review of Physical Chemistry* chapters may be found at http://physchem.annualreviews.org/errata.shtml